INT 182/93 July 1993

# DESCRIPTION OF THE ECRH TRANSMISSION LINE SYSTEM ON TCV

M.A. Henderson, T.P. Goodman, A. Pochelon
& M.Q. Tran

# Description of the ECRH transmission line system on TCV

M.A. Henderson, T.P. Goodman, A. Pochelon, M.Q. Tran
Centre de Recherches en Physique des Plasmas
Association Suisses-Euratom
Ecole Polytechnique Fédérale de Lausanne
21, Av. des Bains 1007-Lausanne/Switzerland

Abstract

A description of the ECRH transmission line system to be installed on TCV is presented. The system is comprised of 9 lines which extend from the TCV Ext. building to the TCV tokamak. Three of the lines are designed at *118GHz* and the remaining at *82.6GHz*. Each element in the line is presented as well as a description of the antennas for both frequencies into the tokamak. The overall efficiency of the line is presented. **All values mentioned are computed from the design of the system as of 1.2.93. This design and computed efficiencies will undergo numerous alterations before the final design is achieved, therefore all information in this report should be viewed as a preliminary design, NOT the realized transmission line system.**

## 1 INTRODUCTION

This report will first discuss the various required elements of the transmission line and show how they will be integrated into the building housing the TCV machine. Each component will be described in the order in which it is encountered in traveling from the gyrotron output window to the entry port on the TCV vacuum vessel. A discussion of the various antennas for launching the wave into TCV follows. The last section presents the total efficiency of the transmission line and concludes the report.

Special note should first be taken that the waveguide size can only be selected once the window design has been finalized. This in turn depends on the specific gyrotrons purchased. For the sake of calculations in this report two guide diameters of *63.5mm* and *88.9mm* were used. These sizes are a reasonable compromise between large-diameter, higher-power, lower-loss waveguide and small-diameter, lower-power waveguide which has better inherent mode filtering and greater tolerance in alignment. In addition, gyrotron frequencies of *82.6GHz* and *118GHz* have been assumed for the X2 and X3 resonant frequencies. The general design principles remain the same even if these values are changed somewhat. Extensive use of the NET/ITER studies [1,2] has been made in this report.

## 2 TRANSMISSION LINE SYSTEM

The proposed ECRH system for TCV will comprise 9 gyrotrons with a total output power of *4.5MW*. There will be 6 conventional gyrotrons, each with an output power of *0.5MW* at *82.6GHz* and 3 tubes operating at *0.5MW* and *118GHz* with the resonator type to be determined. Both gyrotron types are assumed to have gaussian output. Fig. 2.1 illustrates the placement of the 9 gyrotrons and transmission lines with respect to TCV within the tokamak building. A schematic of a typical transmission line is shown in Figs. 2.2(a) and (b). The technology for most components is well developed.

The transmission lines consist of the following components:

1. Waveguide coupler
2. $HE_{11}$ waveguide
3. Miter bends
4. Waveguide switch
5. Miter bend polarizer
6. Calorimeter / Load
7. Waveguide gaps for thermal expansion and isolation breaks

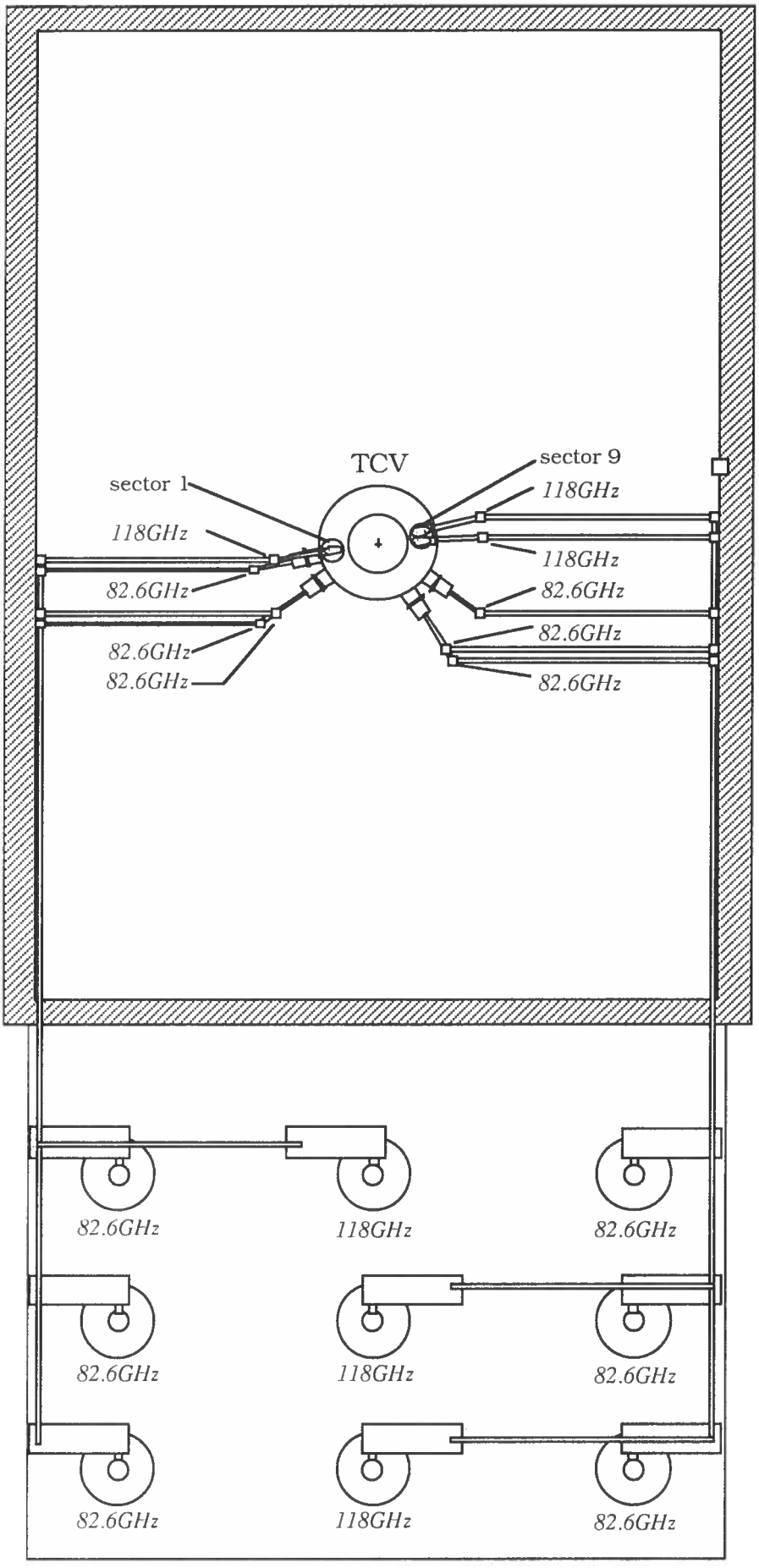


Figure 2.1 Placement of the gyrotrons,transmission lines and TCV.

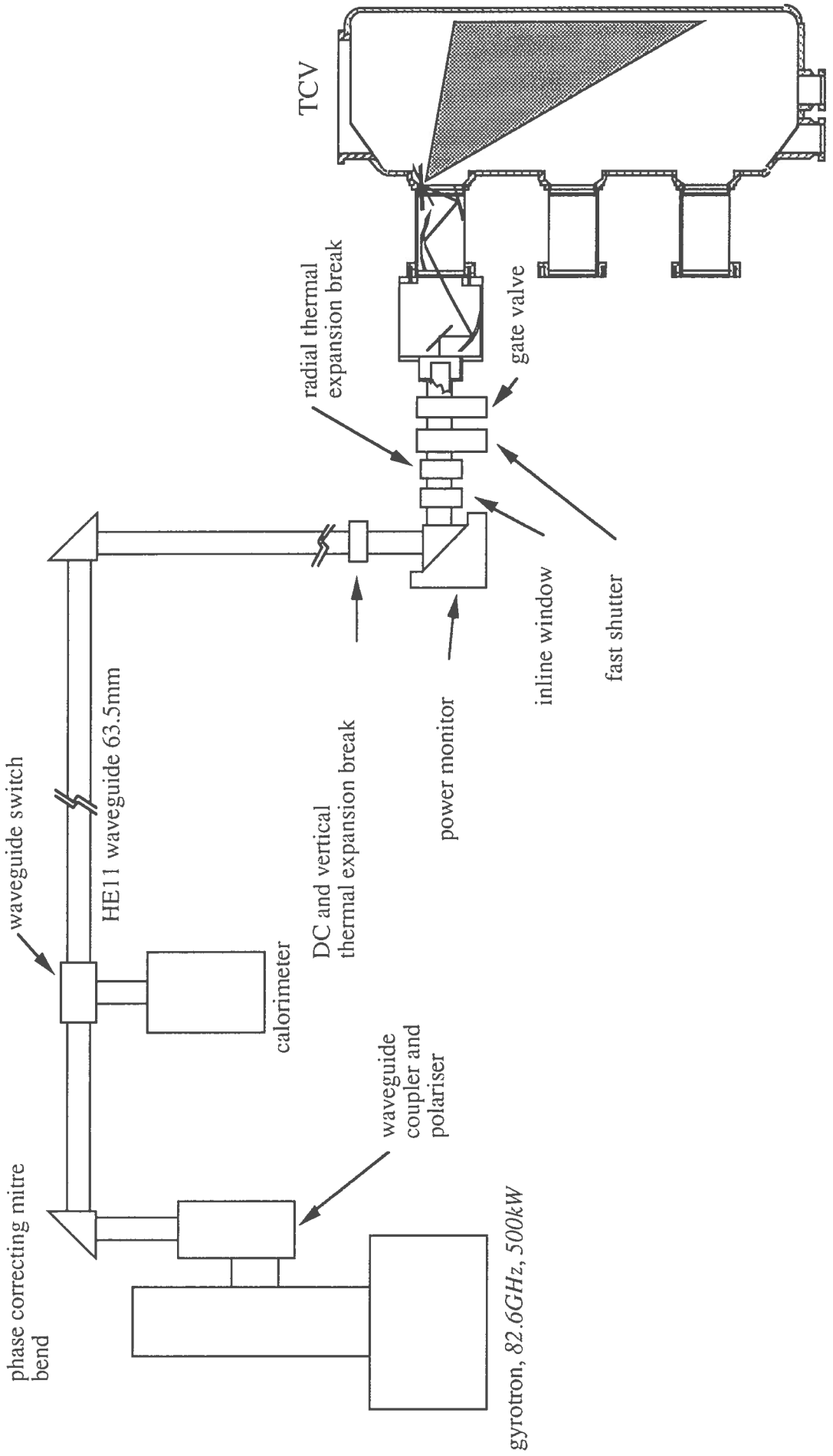


Figure 2.2a Schematic of the 82.6GHz transmission line.

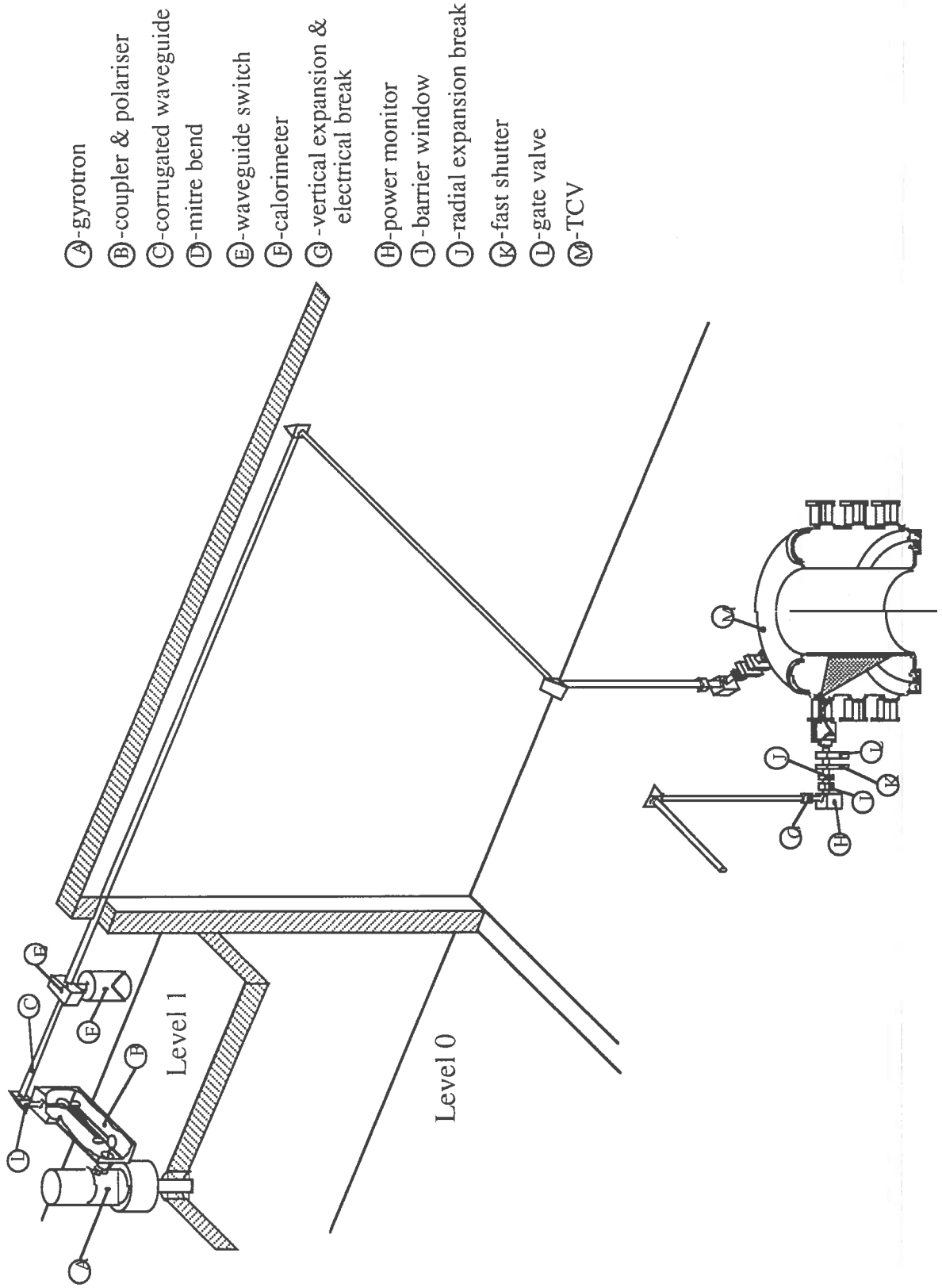


Figure 2.2b View of a typical 82.6GHz transmission line with the individual elements identified.

8 Miter bend power monitor

9 Vacuum window / gate valve

Total losses for the components under discussion are given in each subsection with the losses for the individual components being summarized in Section 3

## 2.1 WAVEGUIDE COUPLER

The output of an *82.6GHz* gyrotron is directly coupled into the $HE_{11}$ waveguide using an elliptical mirror at the output of the gyrotron. The actual design of the mirror is dependent upon the choice of gyrotron and its output spot size and frequency. The mirror couples the $TEM_{oo}$ mode into the $HE_{11}$ mode for propagation in the waveguide with an efficiency of *98.0%* ($\omega_o/a=0.6435$) [3], where $\omega_o$ is the beam waist determined by the radius of the beam at an $e^{-1}$ drop in the electric field and a is the radius of the waveguide.

The design of the elliptical mirror utilizes Gaussian optics [4] in free space. The spot size of the incident and reflected beams are closely matched on the mirror surface, with the spot size $\omega$ at a distance d from the minimum beam waist $\omega_o$ given by:

$$\omega = \omega_o \sqrt{1+\left(\frac{2d}{k\omega_o^2}\right)^2} \qquad (2.1)$$

where $k = 2\pi f/c$ and f is the frequency. The characteristics of the elliptical mirror are determined by matching(aproximately) the phase fronts of the incident and reflected beams at the mirror surface. The focal length, F, of the mirror and the parameters of the ellipse, A and B, are given by:

$$F = \frac{R_1 R_2}{R_1+R_2}, \qquad (2.2)$$

$$A = \frac{R_1+R_2}{2}, \qquad (2.3)$$

$$B = \sqrt{R_1 R_2}\cos(\theta_i), \text{ and} \qquad (2.4)$$

$$C = \sqrt{A^2 - B^2}. \qquad (2.5)$$

In Eqs. 2.2-5, F is the focal length, A,B and C describe the ellipse, and $R_1$ and $R_2$ are the radii of curvature of the input and output beams at distances $d_1$ and $d_2$ from the beam waists given by

$$R_i = d_i\left(1+\left(\frac{k\omega_o^2}{2d_i}\right)^2\right) \tag{2.6}$$

and $\theta_i$ is the angle of incidence of the beam on the mirror. The foci of the ellipse are placed at the center of the two radii of curvature(see Fig. 2.3). The portion of the ellipse used for the mirror is determined by the intersection of the incident beam and the ellipse. The beam is defined by Eq. (2.1) with a radius of the beam on the mirror of $r=2\omega_m$ ($e^{-8}$ in power), where $\omega_m$ is the spot size of the beam on the mirror. For such a radius the intercepted power is 99.9% of the total power of the beam.

The above assumes that the output of the gyrotron will be gaussian. If the pattern is bigaussian a more complicated mirror will be required to optimally match the beam from the gyrotron to the waveguide. Present research being conducted on the *39GHz* gyrotron will prove beneficial in this case.

There are four types of losses associated with the elliptical mirror: ohmic, diffraction, distortion and cross polarization. The fraction of ohmic loss of the power for an E-plane bend is determined by[1]:

$$\frac{P_\Omega^E}{P} = 4s\left(\frac{\varepsilon_o\pi\mu f}{\sigma_{cu}}\right)^{1/2}\frac{1}{\cos\theta_i}, \tag{2.7a}$$

and for an H-plane bend:

$$\frac{P_\Omega^H}{P} = 4s\left(\frac{\varepsilon_o\pi\mu f}{\sigma_{cu}}\right)^{1/2}\cos\theta_i, \tag{2.7b}$$

where

- s = surface roughness factor (typical value = 2) accounting for the anomolously high resistivity at high frequencies
- $\varepsilon_o$ = permitivity of free space ($8.85x10^{-12}C^2/Nm^2$)
- $\mu$ = permeability of free space ($1.0Ns^2/C^2$)
- f = frequency ($Hz$)
- $\sigma_{cu}$ = D.C. conductivity of annealed copper ($5.8x10^7/\Omega m$).

Applying Eqs. (2.7) to a copper mirror:

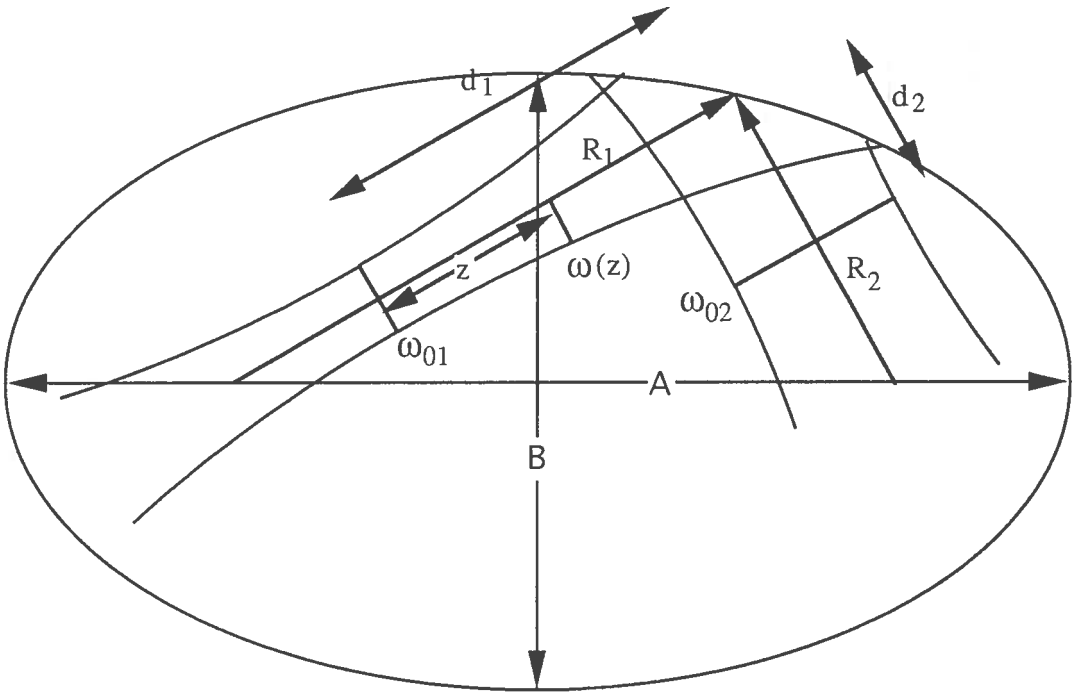


Figure 2.3 A ellipsoid of revolution used to focus a Gaussian beam.

$$\frac{P_{\Omega}^{E}}{P} = (1.752\text{x}10^{-4})\frac{f^{1/2}(\text{GHz})}{\cos\theta_i}, \text{ and} \tag{2.8a}$$

$$\frac{P_{\Omega}^{H}}{P} = (1.752\text{x}10^{-4})\, f^{1/2}(\text{GHz})\cos\theta_i . \tag{2.8b}$$

For the two operating frequencies planned (*82.6GHz* and *118GHz*) the ohmic losses for the coupling mirror are *0.23%*(*0.11%*) and *0.27%*(*0.13%*) (considering $\theta_i = 45°$, and bends in the E-plane(H-plane)).

The losses due to diffraction around the edge of the mirror are given by[1]:

$$\frac{P_d}{P} > \exp\left(-\frac{2a^2}{\omega^2}\right) \tag{2.9}$$

where a is the radius of the mirror. For a typical design value $a = 2\omega$, the associated diffraction loss is *0.1%* . The actual value of a and $\omega$ are dependent upon final selection of both the gyrotrons and the waveguide diameter.

The losses due to the beam distortion(bd) and the cross polarization(cp) resulting upon reflection on the mirror are[5]:

$$\frac{P_{bd}}{P} > \frac{1}{8}\left(\frac{\omega\tan\theta_i}{F}\right)^2 \tag{2.10}$$

$$\frac{P_{cp}}{P} > \frac{1}{4}\left(\frac{\omega\tan\theta_i}{F}\right)^2 \tag{2.11}$$

where F is the focal length of the mirror given by Eq. (2.2). For a typical case with $w_{01}$=*36mm*, $w_{02}$=*28.60mm* and w=*38mm*, using Eqs.(2.1-2,6) the focal length is found to be F=*1031mm(1466mm)* at *82.6GHz(118GHz)*. The corresponding losses in distortion and cross polarization for this case are 0.02(0.01)% and 0.03(0.02)%, respectively.

The total losses for the coupling mirror for the two operating frequency are shown in Table 2.1. An additional 2% loss is added for the coupling into the $HE_{11}$ waveguide[3].

From the calculation of the ohmic losses in the mirror, Eq. (2.7), the maximum temperature rise on the surface of the mirror can be calculated. Assuming no appreciable radial thermal conduction is and considering only the center of the mirror where the power deposition is at a maximum, the maximum (worst case) temperature rise, $\Delta T$, is given by:

$$\Delta T = \frac{t\left(\frac{dP}{dA}\right)_{max}}{\rho_{cu}\, l_m\, c_{cu}}, \qquad (2.12a)$$

where

$$\frac{dP}{dA_{max}} = \frac{2\Delta P_{abs}}{\pi\omega^2}\cos\theta_i \qquad (2.12b)$$

$$\Delta P_{abs} = 4sP\left(\frac{\varepsilon_o \pi \mu f}{\sigma_{cu}}\right)^{1/2} \frac{1}{\cos\theta_i} \qquad (2.12c)$$

and

$\Delta P_{abs}$ = absorbed power on the mirror
$\rho_{cu}$ = density of copper (8.96 g/cm$^3$),
$c_{cu}$ = specific heat of copper (0.385 J/gK),
$l_m$ = thickness of mirror (minimum value of 0.5 cm),
t = pulse length (2 sec.),
P = gyrotron output power (500 kW).

| Losses | 82.6 GHz | 118 GHz |
|---|---|---|
| Ohmic | 0.23% | 0.27% |
| Diffraction | 0.10% | 0.10% |
| Distortion | 0.02% | 0.01% |
| Cross Polarization | 0.03% | 0.02% |
| Coupling | 2.00% | 2.00% |
| Total | 2.38% | 2.40% |

Table 2.1 Losses asociated with the elliptical mirror for coupling into the $HE_{11}$ waveguide.

Using the values mentioned previously and Eqs. (2.12) the maximum temperature rise on the mirror surface is calculated to be *40.7°C(82.6 GHz)* and *48.6°C(118 GHz)*. The average temperature rise on the surface of the mirror can be calculated by substituting the average power density absorbed on the mirror for the max. power density(Eq. 2.12b). The average power density is given from:

$$\left(\frac{dP}{dA}\right)_{ave} = \frac{\Delta P_{abs}}{4\pi\omega^2}\cos\theta_i\,. \qquad (2.12d)$$

Using Eq. (2.12d) the average temperature rise on the surface of the mirror for the two frequencies is *5.1°C* and *6.1°C*. Considering a duty cycle of *10min* there is sufficient time for the equalization of the thermal distribution throughout the mirror. Assuming the mirror is only cooled radiatively and is within a vacuum, the maximum steady state temperature averaged over the surface of the mirror is given by(Stefan's law):

$$T = \left( T_o^4 + \frac{\Delta P_{abs}\tau}{8\pi\omega^2\varepsilon\sigma\cos\theta_i} \right)^{\frac{1}{4}} (K). \qquad (2.13)$$

where

$T_o$ = temperature of surrounding media (*303K*),
$\tau$ = duty cycle(*0.33%*)
$\varepsilon$ = emissivity of copper (0.1, for polished Cu).

Using Eq. (2.13), the maximum steady state temperature of the coupling mirror is less than *120°C* for either frequency. This temperature is well within the thermal range of the mirror and will present no technical difficulties. This maximum could be lowered by the addition of a carbon backing to increase the emissivity from 0.1 to 0.7-0.9 over half of the area. For the choice of a non evacuated line, the maximum temperature will be much less due to the increased convection losses.

## 2.2 $HE_{11}$ WAVEGUIDE

Corrugated waveguide is used as a consequence of its low ohmic wall losses for the $HE_{11}$ mode, high power handling capability and broad band characteristics. In addition, the radiated beam couples well to the fundamental gaussian free-space $TEM_{00}$ mode. For small diameters, the waveguide has, moreover, been shown to provide good mode filtering since ohmic wall losses are significant for higher order modes. In particular, groups of miter bends connected by *2m* sections of *31.8mm* diameter aluminum guide have been shown to be free of trapped modes over a 500 MHz bandwidth at *110GHz* [6]. The presence of symmetrical gaps along the axis of $HE_{11}$ guide exhibit low losses in coupling to higher order modes. Gaps are therefore used for electrical isolation and thermal expansion compensation. They are also employed in waveguide switches. For a nominal waveguide diameter of *63.5mm* (*2.5"*) is taken as an example; the final size being determined by window compatibility. This waveguide has a power-handling capability of *>1MW* (STP) and is flooded with dry $N_2$ or $CO_2$, especially at *118GHz*, to avoid the $O_2$ absorption peak in air near this frequency. The use of an evacuated waveguide is also an alternative pending the choice for the window near TCV.

The corrugation dimensions are optimized for minimal power losses at both operating frequencies. The groove depth is optimized according to the theory by Doane[7] for the two different operating frequencies so that the same waveguide can be used for either X2 or X3 transmission. The attenuation of the waveguide as a function of frequency is shown in Fig. 2.4a for the two most likely choices of waveguide size (a=*31.75* and *44.45mm*) and a corrugation groove depth, d, of*0.812mm* (see Fig. 2.4b). It can be seen that the attenuation decreases with

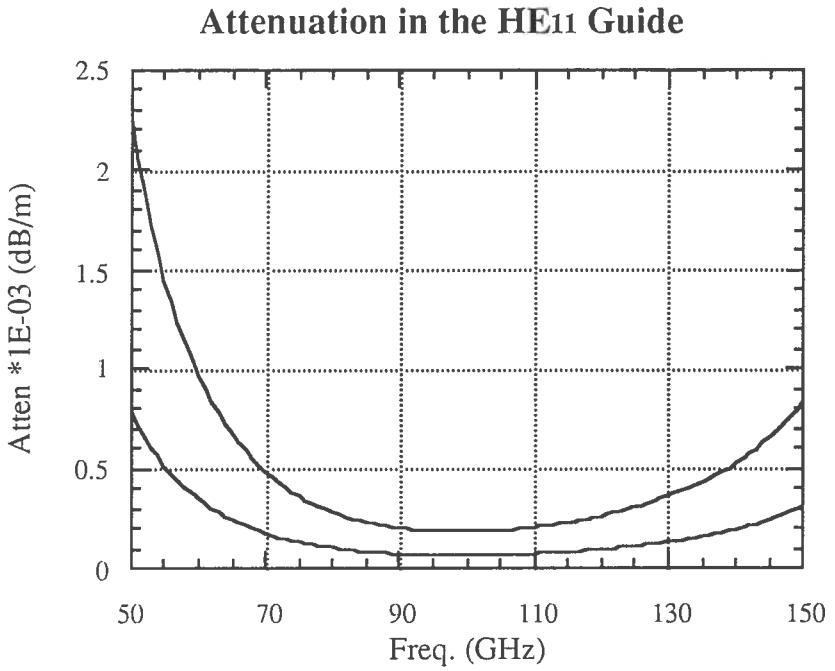


Figure 2.4a Attenuation in the HE11 guide for two different waveguide diameters.

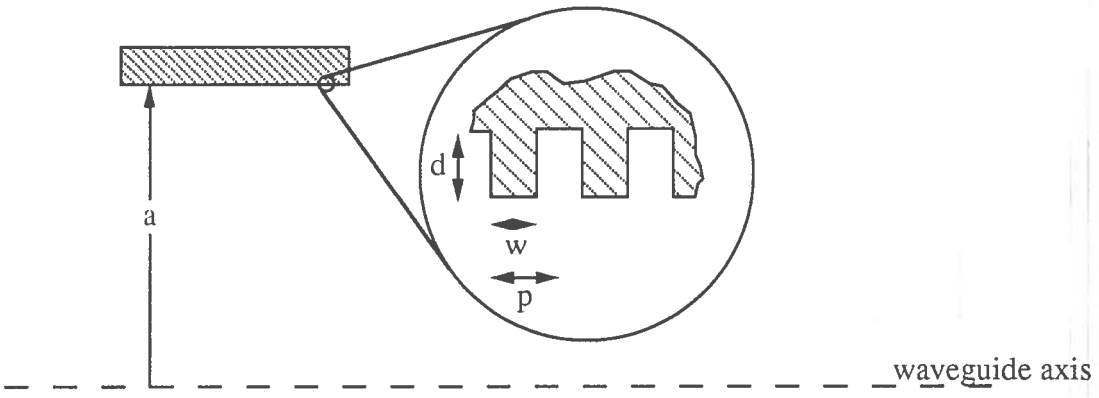


Figure 2.4b Cross section of the HE11 waveguide.

increasing diameter. The ratio of the width of the grooves to the period is set at 0.5. The period(p) of the grooves must remain small in relation to the wavelength but must be large enough to be machined. Values of $p < (0.3 \text{ to } 0.4)\lambda$ have been shown to be well described by the theory set forth in Doane. If the width(w) of the corrugations is chosen smaller than the groove depth then the excitation of higher-order standing-waves in the corrugations will be prevented. With w=0.9d(0.8d) the attenuation in the evanescent first higher-order mode is *12.5dB(18dB)*. With p=*1.016mm*($p<0.4\lambda$ at *118GHz*) the width of the grooves becomes *0.508mm* or $0.63\lambda/2(0.28\lambda/2)$ at *118GHz(82.6GHz)*.

The efficiency of the line at the two operating frequencies can be obtained from Fig. 2.4a. For *82.6GHz(118GHz)* the loss is $9.15x10^{-5}dB/m(8.98x10^{-5}dB/m)$ for a=*44.45mm* and $2.50x10^{-4}dB/m$ $(2.46x10^{-4}dB/m$ )for a=*31.75mm*. An estimated path length of approximately *30m*, with a=*44.45mm(31.75mm)*, yields a loss of *0.063%(0.17%)* at *82.6GHz* and *0.062%(0.17%)* at *118GHz* per line.

The material chosen and method of construction for the $HE_{11}$ waveguide will be determined by the type available commercially at the time of purchase.

The magnitude of the electric field within the waveguide is given by[7]:

$$|E| = \frac{1}{a}\sqrt{\frac{2\,P\,Z_o}{\pi}}\,\frac{J_0(2.405\,\frac{r}{a})}{J_1(2.405)}, \qquad (2.14)$$

where $Z_o$ is the impedance of free space ($= \sqrt{\frac{\mu_o}{\varepsilon_o}} = 376.8\Omega$) and P is the total power. The maximum field strength in the waveguide for a radius of *44.45mm(31.75mm)* is *4.75kV/cm(6.65kV/cm)*. For the smaller radius the maximum field strength is approximately 1/4 the breakdown field intensity in air at *1ATM* and *20°C*. The maximum power density within the waveguide is given by:

$$\left(\frac{P}{A}\right)_{max} = \frac{P}{\pi a^2}\,\frac{J_0^{\,2}(2.405\,\frac{r}{a})}{J_1^{\,2}(2.405)}. \qquad (2.15)$$

For the given radius *44.45mm(31.75mm)* the maximum power density is $29.9kW/cm^2(58.7kW/cm^2)$.

Losses associated with the waveguide include misalignments, bends, etc. For misalignments at a junction of two waveguides(corresponding to an axial displacement of $\Delta a$) the power coupled into other modes is described by[1]:

$$\frac{P_{rd}}{P} = 1.071\left(\frac{\Delta a}{a_o}\right)^2, \tag{2.16}$$

where $P_{rd}$ is the total power coupled into other modes due to the radial displacement and $a_o$ is the radius of the waveguide. The above equation represents the losses coupled into $TE_{01}$ and $HE_{21}$(H-plane) and $TM_{02}$ and $HE_{21}$(E-plane). The losses associated for a *1.0mm* displacement for the two waveguide diameters under consideration, a=*31.75mm* and *44.45mm*, are *0.12%* and *0.059%* respectively. These values are small even though the magnitude of the displacement is larger than can be expected and can, therefore, be neglected. Note the above equation is independent of frequency provided the guide is far from cutoff.

Other losses which decrease with an increase in radius are abrupt changes in radius($P_{ra}$) and abrupt elliptical offsets ($P_{re}$) due to absolute fabrication tolerances. These are found from the following equations[1]:

$$\frac{P_{ra}}{P} = 1.156\left(\frac{\Delta a}{a_o}\right)^2, \tag{2.17}$$

for $HE_{1n}$ modes, and

$$\frac{P_{re}}{P} = 0.36\left(\frac{\Delta a}{a_o}\right)^2, \tag{2.18}$$

for $HE_{31}$ mode(the most likely higher order modes). Considering $\Delta a$=*1.0mm* for the above two equations, the losses for $P_{ra}$ and $P_{re}$ for a=*44.45mm*(*31.75mm*) are found to be *0.59%*(*0.12%*) and *0.02%*(*0.04%*) respectively. Again these values are small considering the large magnitude of the displacement.

Losses which increase with increasing radius are mainly those resulting from angular alterations introduced in the line. The two most significant are abrupt tilts at the junction of two waveguides ($P_{at}$) and unintentional curvature of the waveguide due to sagging ($P_{ar}$). These losses are described by [2.8]:

$$\frac{P_{at}}{P} = 0.0543\ (\text{ka}\ \theta[rad])^2, \tag{2.19}$$

and

$$\frac{P_{ar}}{P} \propto \left(\frac{ka}{R}\right)^2, \tag{2.20}$$

for $TE_{01}$(H-plane), $TM_{02}$(E-plane) and $HE_{21}$ modes. Where $\theta$ is the angle between the different waveguide axes and R the radius of curvature of the of the sagging waveguide. For the angular tilt between waveguides, consider a misalignment of a *1.0mm* displacement over *1.0m*: $\theta$ = *0.001rad*. With a=*44.45mm*(*31.75mm*) the abrupt tilt losses are *0.32%*(*0.016%*) and

*0.066%(0.033%)* for the two frequencies *82.6GHz* and *118GHz* respectively. The constant of proportionality in Eq. 2.20 was determined from the example in the ITER report and was found to be $1.76 \times 10^{+05}$. This value should not be assumed accurate and yields only and order of magnitude estimate for the error. Assume a sag of *1mm* over a *2mm* long waveguide(R=*500m*) with the ends fixed, this corresponds to the equivalent of a *0.001rad.* tilt. With this value the losses with a=*44.45mm(31.75mm)* are *0.42%(0.21%)* and *0.85%(0.43%)* for the two frequencies *82.6GHz* and *118GHz* respectively. Note that out of all the sources of losses the later two are the most sensitive and great care should be taken in preventing these types of misalignments when supporting the waveguide.

The final choice of the waveguide diameter is dependent more on financial optimization then on the optimization of the efficiency of the line, provided unintentional sagging can be avoided. The use of an evacuated line with a smaller diameter insures low losses; however, the cost of the pumping and related vacuum equipment must be weighed against the cost of the window at the TCV side(Sec.2.9) and a more rigid support system. Also influencing the choice, is the availability and cost of the guide. At present this decision has not been made and is deferred until after support has been approved.

To ensure correct alignment of mirrors and miter bends, the lines are aligned with a laser beam passing inside the guide. Since additional losses can be introduced due to unintentional curvature induced by the waveguide sagging between supports, all waveguide mounts are also laser aligned, external to the waveguide.

The support structure for the waveguide has not been fully envisioned; however, required tolerances for the system can be obtained from the above equations. The support structure will consist of two types of supports: mounts and columns. The mounts will be positioned at short intervals along the waveguide and will directly support the waveguide insuring minimal bends and displacements. The columns will support the structure to which the mounts are affixed. The columns need not be aligned with the same accuracy as the waveguide, since the mounts will allow small adjustments in positioning the waveguide. The displacement from the center of the waveguide between successive mounts will be limited to *1mm* over a *2m* length, recalling that the largest losses were due to sagging of the waveguide and angular misalignments between two waveguide pieces. Assuming that the waveguide will be supplied in lengths of *2m* or greater and each waveguide will be mounted at intervals of approximately*1m*, this corresponds to a maximum displacement of *0.5mm* between mounts. The tolerances are specified for the larger diameter waveguide, if the smaller diameter guide is chosen these tolerances will be relaxed such that the same efficiency is maintained.

## 2.3 MITER BEND

In the case of highly overmoded waveguides, compact, low-loss changes in waveguide direction can be made with phase-correcting miter bends(see Fig. 2.5). The phase-correcting curved mirror decreases the power coupled to higher order modes by 1/2 compared with plane mirrors [8]. The phase corrected mirror matches the phase fronts from the waves propagated from the waveguides on either side of the mirror. The design of the phase corrected mirror will follow the description set forth by Vaganov[9].

The mode converted losses for a phase corrected miter bend are approximated by [8]:

$$\frac{P_c}{P} = 0.15\left(\frac{\lambda}{a_o}\right)^{3/2}. \qquad (2.21)$$

Approximately one third of the power in the coupled modes is reflected and two thirds transmitted. An H-plane phase corrected bend results in slightly lower coupled losses, *96%* of the equivalent E-plane bend. The related ohmic losses of the miter bends are determined from Eqs. 2.8. Each transmission line will be comprised of 1 H-plane and 1 E-plane phase corrected bend, and 2 E-plane non phase corrected bends. The 2 non phase corrected bends will each have incorporated into the mirrored surface of the bend a grating which will act as a universal polarizer (see Sec. 2.5). The total losses for all the bends are shown in Tables 2.2a and b. The ohmic losses above will be slightly decreased by silver coating the mirrors. The high reflectivity of the silver coating is also an advantage, since all mirrors need to be polished to allow laser alignment.

The maximum and average temperature rises on the miter bend mirror can be calculated from Eqs. 2.12. Considering the smallest waveguide diameter($\omega$=*20.431mm*) which has the largest power density, the maximum temperature rise is *140°C*(*168.2°C*) for *82.6GHz*(*118GHz*). The above is for a worst case scenario assuming no thermal conduction away from the mirror during the shot. Both temperatures are within the thermal limits of copper. The average temperature rise of the miter bend mirror is *17.5°C*(*21.0°C*). The average power density absorbed in the mirror is *15.17W*(*18.14W*). This power can be easily radiated away with an addition of a radiator fin on the back of each bend, assuming that the line itself proves to be an insufficient heat sink/radiator.

The peak power density on the miter bend is obtained from the power density of the $HE_{11}$ mode as described by Eq. 2.15. The area of the miter bend is slightly enlarged due to the incident angle which modifies Eq. 2.15 as follows:

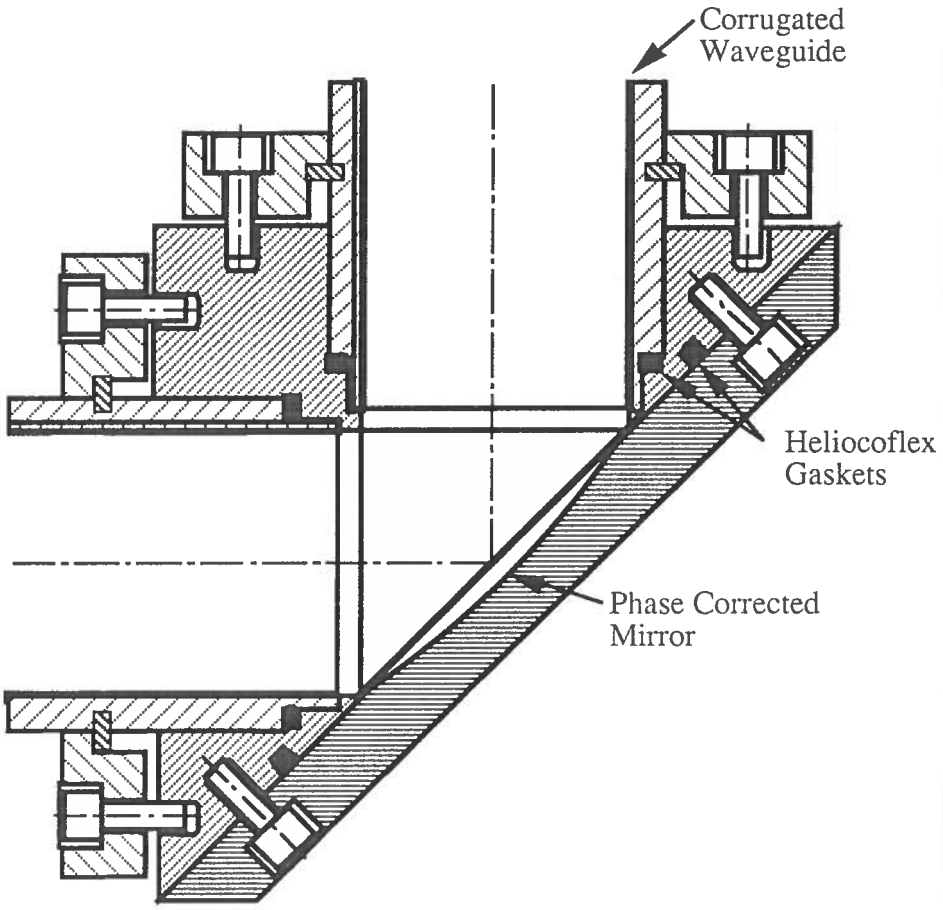


Figure 2.5 Drawing of the phase corrected miter bend.

$$\left(\frac{P}{A}\right)_{max} = \frac{P\cos\theta}{\pi a^2}\,\frac{J_o^{\,2}(2.405\,\frac{r}{a})}{J_1^{\,2}(2.405)}. \qquad (2.22)$$

For a waveguide radius of *44.45mm(31.75mm)* the peak power density at the surface of the miter bend is *21.1kW(41.4kW)*.

| Miter bend Type(82.6GHz) | # | $P_\Omega$ | $P_c$ | $P_t$ per Bend | $P_t$ |
|---|---|---|---|---|---|
| H-plane w/phase Cor. | 1 | 0.11% | 0.34%(0.56) | 0.45%(0.67) | 0.45%(0.67) |
| E-plane w/phase Cor. | 1 | 0.23% | 0.34%(0.56) | 0.57%(0.79) | 0.57%(0.79) |
| E-plane | 2 | 0.23% | 0.68%(1.12) | 1.11%(1.35) | 2.21%(2.7) |
| Total losses | | 0.80% | - | - | 3.2%(4.1) |

Table 2.2a The losses associated with the miter bends in the *82.6GHz* transmission line with a=*44.45mm(31.75mm)*.

| Miter bend Type(118GHz) | # | $P_\Omega$ | $P_c$ | $P_t$ per Bend | $P_t$ |
|---|---|---|---|---|---|
| H-plane w/phase Cor. | 1 | 0.13% | 0.20%(0.33) | 0.33%(0.46) | 0.33%(0.46) |
| E-plane w/phase Cor. | 1 | 0.27% | 0.20%(0.33) | 0.47%(0.60) | 0.47%(0.60) |
| E-plane | 2 | 0.27% | 0.40%(0.66) | 0.67%(0.93) | 1.34%(1.85) |
| Total losses | | 0.94% | - | - | 2.13%(2.89) |

Table 2.2b The losses associated with the miter bends in the *118GHz* transmission line with a=*44.45mm(31.75mm)*.

## 2.4 WAVEGUIDE SWITCH

A waveguide switch[1](see Fig. 2.6) placed after the first miter bend allows the beam to be diverted to a calorimeter for power measurements. The switch will incorporate a phase corrected mirror as in the miter bends for minimal losses. For transmission to TCV the switch

will allow straight transmission. The losses associated with the switch in the unswithched(straight through) position will be due to the gaps between the waveguide of the switch and the line and those due to misalignment of the two guides. Of the misalignment losses mentioned in Sec. 2.2, angular misalignements between the switched waveguide and the fixed waveguide produce the greatest losses. Therefore, the switch will need to be aligned with the same accuracy as two successive waveguide pieces and insure the integrity of the alignment is maintained after multiple switchings. The losses due to a gap in the waveguide are given by[1]:

$$\frac{P_g}{P} = 0.29\left(\frac{L\lambda}{2a^2}\right)^{3/2}, \qquad (2.23)$$

where L is the length of the gap and $\lambda$ is the wavelength of transmitted microwaves. With the suggested gap between the two guides of $\lambda/6$, the losses are negligible. Therefore the presence of the switch will minimally effect the beam transmission with essentially zero losses.

The switch also provides operational safety at the tokamak since its positioning is integrated with the computer control system and must be in the "diverted" position before access to the tokamak is granted.

## 2.5 MITER BEND POLARIZER

Two of the miter bends within the line will have the phase corrected mirror replaced with a grating to allow polarization of the beam. The miter bend polarizers[10] will allow the adjustment of the polarization of the beam to provide optimum matching with the plasma. The polarizers will be designed following the work of Smits[11] and will consist of a plane and elliptical polarizer in series to provide a wide range of polarizations. The polarizer will be designed at the CRPP using in-house experience in the design of gratings used for quasi-optical gyrotron cavities [12].

The losses associated with the polarizers will be slightly larger due to the lack of a phase corrected surface(see Tables 2.2). The ohmic losses will be equivalent to the E-plane miter bends described above.

An alternative design to the miter bend polarizers is to incorporate the polarizers in with the waveguide coupler described in section 2.2. This alternative introduces two extra plane grating mirrors(the polarizers) and an additional elliptical mirror(see Fig.2.7). The advantages of this design is an increased number of obtainable polarization configurations and a potential

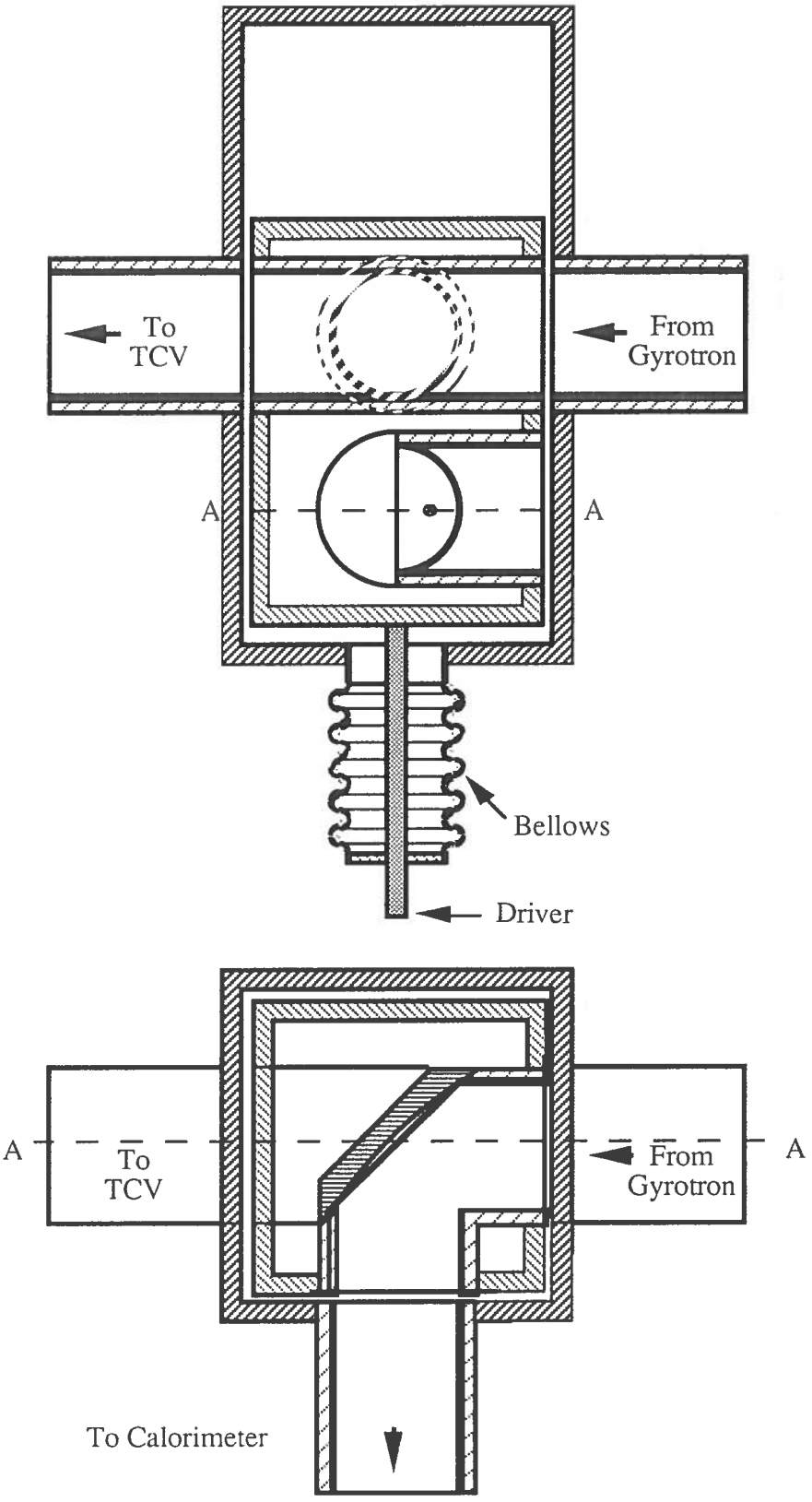


Figure 2.6 Drawing of the waveguide switch.

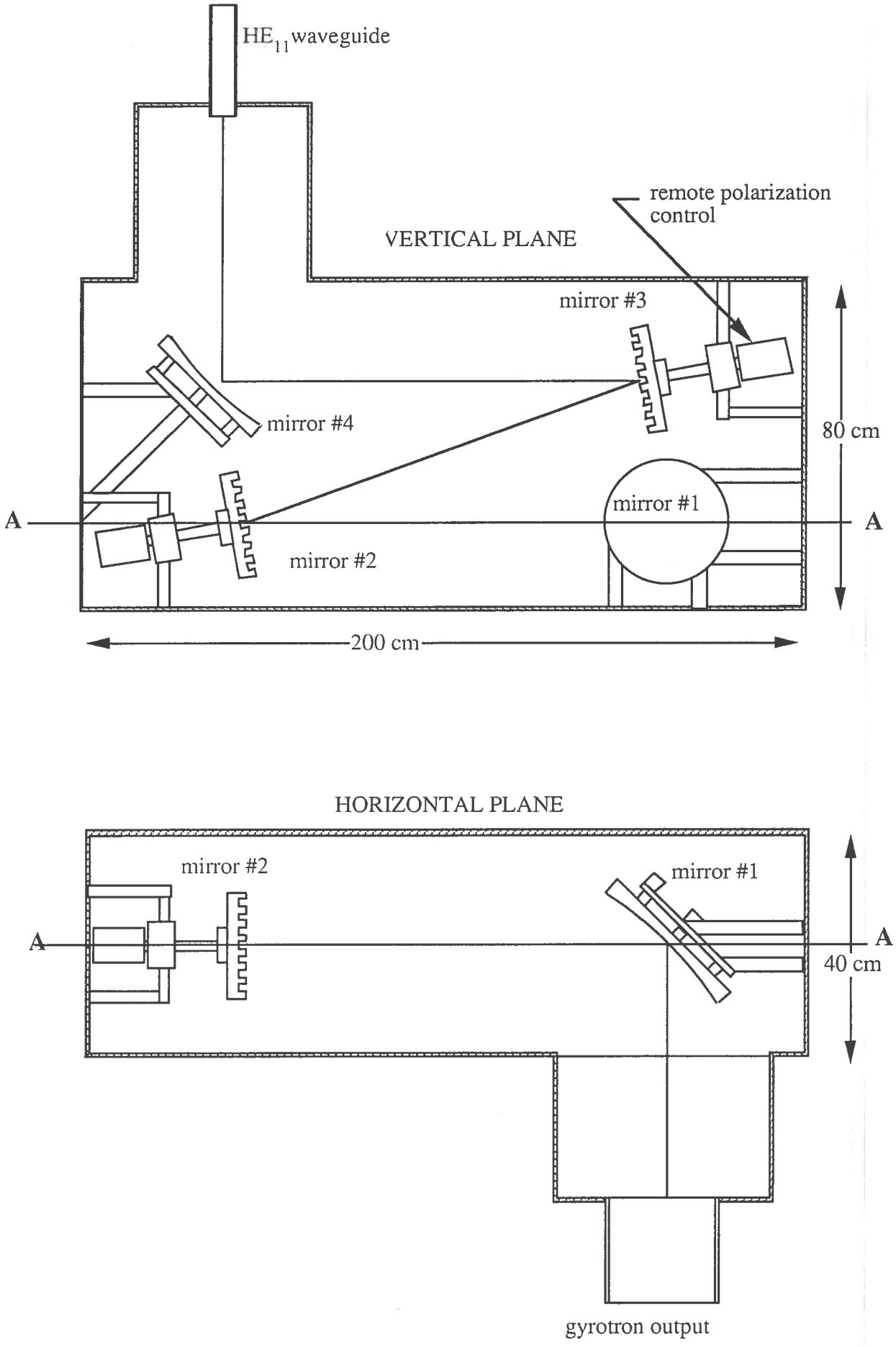


Figure 2.7 Drawing of the waveguide coupler with polarizer system.

reduction of the losses in the transmission line depending on the chosen diameter of the waveguide. The alternative design uses a similar elliptical mirror at the output of the gyrotron as described before. However instead of directly matching into the waveguide the elliptical mirror refocuses the beam in free space. Two plane gratings are placed symmetrical about the beam waist with as small of an incident angle as possible. A second elliptical mirror is placed after the last polarizer to properly couple the expanding beam into the waveguide. The efficiency of such a system is shown in Table 2.3 and is essentially independent of waveguide diameter.

A comparison of the two polarizer systems is also shown in Table 2.3. The alternative design slightly reduces the losses for the *82.6GHz* line which when included with the greater range of polarizations available, makes the alternative design favorable. For the *118GHz* case, the alternative design produces greater losses and therefore should not be applied to this line. Furthermore, the X3 transmission line will only require a plane polarizer which further reduces the losses for the original miter bend design.

| | 82.6 GHz a=*44.45mm* | 82.6 GHz a=*31.75mm* | 118 GHz a=*44.45mm* | 118 GHz a=*31.75mm* |
|---|---|---|---|---|
| Additional Elip. mirror | 0.38% | 0.38% | 0.4% | 0.4% |
| 2 plane grating mirrors | 0.52% | 0.52% | 0.55% | 0.55% |
| 4 phase corrected E-plane miter bends | 2.26% | 3.12% | 2.83% | 2.38% |
| Total losses for the polarizer w/coupler | 3.14% | 3.99% | 2.83% | 3.33% |
| Polarizer w/miter bend | 3.2% | 4.1% | 2.13% | 2.89% |

Table 2.3 Comparison of the losses for the two polarizer designs with a=*44.45mm*(*31.75mm*).

## 2.6 CALORIMETER

A microwave calorimeter, to be built in-house or purchased externally, is installed at the waveguide switch and used to corroborate power monitor measurements made just before entry into the TCV vessel (see Section 2.8). A dummy load can also be placed at this location during long-pulse testing of the individual gyrotrons. Only one calorimeter for each frequency is

required because the layout of the gyrotrons allows easy displacement of the calorimeter from one line to the next. The calorimeter/dummy loads should not present any major technical difficulties.

## 2.7 THERMAL EXPANSION AND ELECTRICAL ISOLATION BREAKS

Since it will be possible to operate TCV at various temperatures, the vacuum vessel will shift radially and vertically due to thermal expansion. Two joints are therefore introduced in the transmission line near TCV to accommodate such displacements, without disturbing the line integrity. The first is placed in the vertical section just before the power monitor. Electrical isolation is provided in this joint to separate the rest of the transmission line from TCV. The second, located just before the gate valve, compensates for radial displacements. Both joints will have a nominal gap of *10mm* to compensate for shifts of *±5mm*. The associated losses per joint are calculated from Eq. (2.23). For waveguide with a radius of *44.45mm*(*31.75mm*) the losses due to a *10mm* gap is *0.026%*(*0.077%*) for *82.6GHz* and *0.015%*(*0.041%*) for *118GHz*.

## 2.8 POWER MONITORS

A power monitor [1] to measure both the transmitted and reflected power is incorporated in the last miter bend before the vacuum window and antenna system of each line. This also permits a final measure of the polarization for each shot. The details of the power monitored can be obtained from the ITER report.

## 2.9 VACUUM WINDOW

A vacuum window for the end of each line is to be purchased from the gyrotron manufacturer. Three possibilities are: 1) inertially-cooled windows, 2) cryogenic edge-cooled windows and 3) double-disk, face-cooled sapphire windows. The loss associated with the window are unknown until the final selection of the window type. However a *2%* loss is assumed until that date.

A fast shutter and a gate valve are positioned between the window and the antenna system to isolate the window during torus baking and vessel conditioning. For a window incorporated in the waveguide, a valve with a *15mm* gap has a coupling loss(see Eq. 2.23) of $0.047\%(0.129\%)$ at $82.6GHz$ and $0.027\%(0.075\%)$ at $118GHz$ for a radius of $44.45mm(31.75mm)$.

## 3 TCV ANTENNAS

A description of the two different antenna designs are described in this section. The first antenna design is for the second harmonic X-mode heating at *82.6GHz* and is to be placed on TCV's lateral ports. The second antenna design is for the third harmonic X-mode heating at *118GHz* and is to be placed on the 'manhole' ports atop TCV.

### 3.1 X2 ANTENNAS

Second Harmonic X-mode (X2) heating and current drive will be carried out from the upper lateral (4) and equatorial (2) ports. As discussed in the Phase I report, these ports provide the best access and absorption characteristics for the various plasma configurations which can be produced in TCV. The antenna structure discussed below has been designed to meet or exceed the following geometric requirements for the microwave beam:

1 poloidal rotation to provide line-of-sight access to the plasma center for configurations I through III (see Fig. 3.1) i.e. $\theta_p = 7^o–55^o$ from the horizontal;

2 toroidal rotation of $\theta_t = \pm 40^o$;

3 beam divergence $\leq 3^o$ ($\theta_{div} = \text{atan}(\omega(z)/R(z))$ where $\omega$ is the beam spot radius ($e^{-1}$ E-field), R is the radius of curvature of the phase front, and z is the distance between the heating point and the beam waist along the beam trajectory).

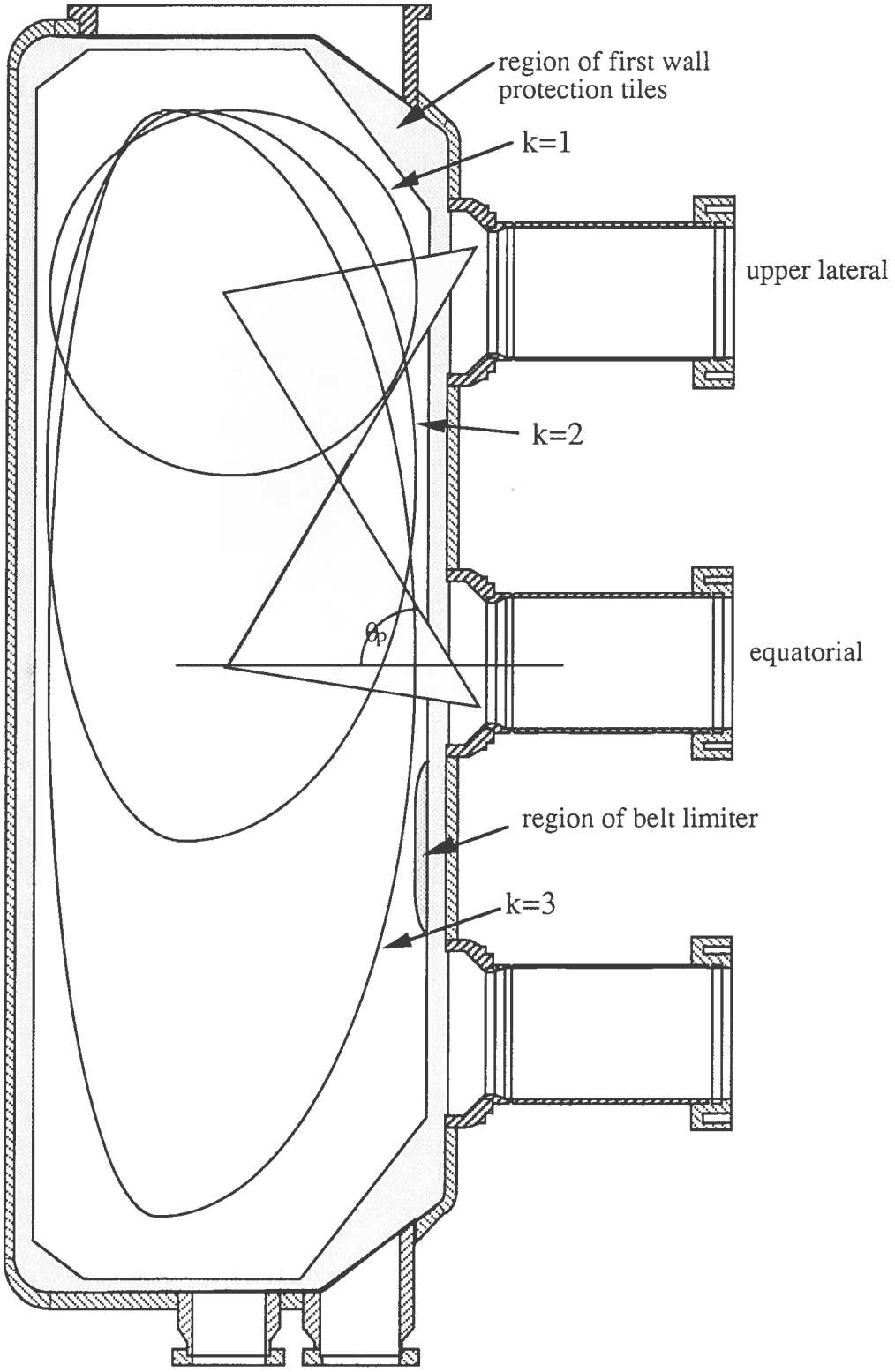


Figure 3.1 Poloidal cross section of TCV, showing the required X2 accessibility.

In addition, overall TCV operation requires:

4 utilization of the existing ports with the addition of port extensions which will be limited in size by the field coils and their support structures;

5 minimization of plasma contamination with high-Z ions from the antenna structure.

It should also be noted that the antenna system should be modular to allow it's use in both the equatorial and upper lateral ports.

### 3.1.1 QUASI-OPTICAL MIRROR SYSTEM

The X2 antenna is comprised of 4 mirrors(see Fig. 3.2) which transfers the beam from the end of the waveguide into the plasma at various poloidal and toroidal angles. The antenna is comprised of two elliptical and two plane mirrors. The incoming waveguide is coaxial with the lateral port. An elliptical mirror is placed in front of the open ended waveguide which reflects the beam at a $90°$ angle. The placement of the first mirror facilitates the rotation of the whole assembly about the axis of the port thus giving the freedom to change the toroidal launching angle. Next a plane mirror reflects the beam into the port with as shallow an angle as possible. The third mirror is elliptical and refocuses the beam such that the beam waist is projected as far as possible into the plasma. The fourth mirror is a plane mirror that pivots in the plane of the beam trajectory providing the poloidal rotation. A brief description of the design follows.

The process of designing the X2 antenna was achieved through several iterations of optimizing the design. There are ten critical restrictions in the design of the antennas which arise from the limited space of the lateral port. The restrictions are identified in Fig. 3.3 and are briefly described below:

1) Vertical position of mirror 4 within the neck of the lateral port.
2) Vertical position of the mirror 3 for clearance during axial rotation of the mirror assembly.
3) Beam clearance with the vessel wall when heating elongated plasmas.

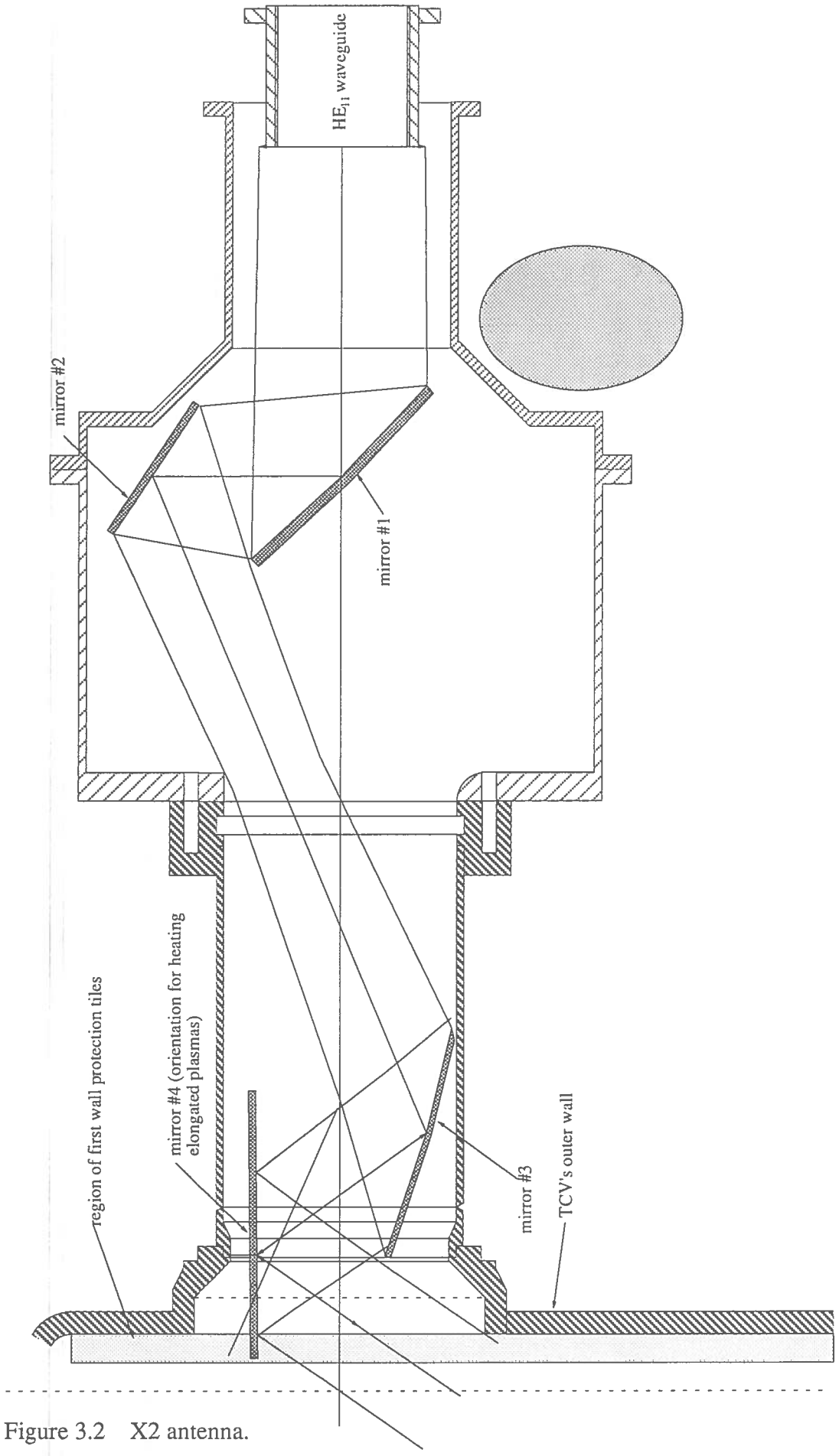


Figure 3.2 X2 antenna.

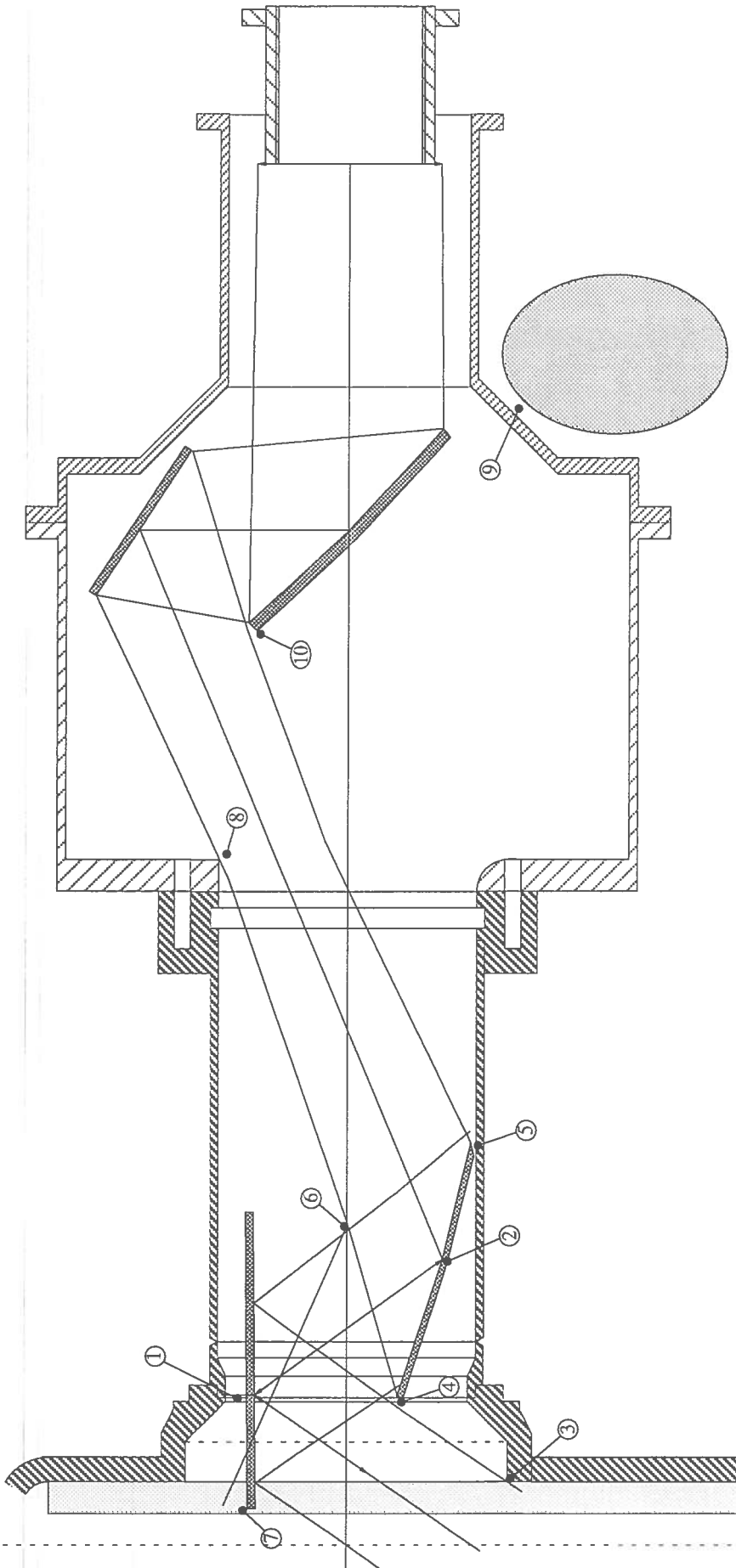


Figure 3.3 X2 antenna with critical points identified.

4) Clearance of the radially inward edge of mirror 3 with the beam when heating elongated plasmas.
5) Clearance of the radially outward edge of mirror 3 with the base of the lateral port.
6) Clearance of the radially outward edge of mirror 4 for circular plasma heating with the beam incident on mirror 3.
7) $>2cm$ clearance between the radially inward edge of mirror 4 for any rotation and the plasma boundary.
8) Clearance of the beam between mirrors 2 and 3 with the corner of the end of the port.
9) Clearance of the mirror(and port extension) with the TCV support structure and the toroidal field coils.
10) Clearance of the radially inward edge of mirror 1 and the outward edge of the beam between mirrors 2 and 3.

The design of the antenna system proceeded in the opposite direction as the direction of propagation and will be described in a similar fashion starting with mirror 4 and proceeding with each restriction as ordered above.

The vertical placement of the front surface of mirror 4 is limited by the choice of the beam spot size incident on the mirror surface. A spot size of $\omega_4=22.7mm$($e^{-1}$ in E-field) was set as the smallest value allowable to limit the increase of the power density incident on the surface of a mirror. The maximum power density at the mirror surface is given by Eq. 2.12d:

$$\left(\frac{dP}{dA}\right)_{ave} = \frac{2P}{\pi\omega^2}\cos\theta_i \ .$$

For the above value of $\omega_4$, this corresponds to a peak power density of $43.7kW/cm^2$. Mirror 4 (mirror diameter of $4\omega_4$) is raised until there is a $3mm$ clearance on either edge from the port wall. This placement corresponds to a height of $z'=57mm$, where z' is measured from the axis of the lateral port. The rotation of the mirror for the elongated heating case(case A) was optimized iteratively to be $+0.5°$ above the horizontal. The angle was determined from limiting the incident angle for the circular heating case(case B) to less than $60°$ and projecting the incident beam on mirror 4 as far radially outward as possible. The reflected beam angle was determined to be $55°$ by raytracing techniques of the beam into the plasma(TORAY codes, A. Pochelon).

Larger angles underwent a greater diffraction through the plasma such that at angles greater than *55°* less than *70%* of the beam reaches the resonance layer.

The second constraint, the vertical placement of mirror 3, is chosen by balancing the size of the mirror with the distance from mirror 4. The larger the distance between the two mirrors the larger the distance the beam waist can be projected into the plasma and the larger the angle for the incident beam on mirror 3. Again through an iterative method the optimum spot size on mirror 3 is chosen to be *25.25mm* with just over *2mm* clearance on both edges. The height of the third mirror is z'=*-59.5mm* and the distance between the two mirrors is *144mm*(for the case A). The characteristics of the reflected beam from mirror 3 is determined from the knowledge of the spot sizes on the two mirrors and the distance between them. Using the equations for the beam propagation(Eqs. 2.1,6) the beam waist in the plasma is found to be *22.261mm* at a distance of *254.65mm* after the third mirror.

Considering the rotation of mirror 4 for case A, the path of the beam after the fourth mirror can be described. Both mirrors are now radially displaced so that the reflected beam just clears the edge of the joint formed at the base of the lateral port and the VV, point 3 (see Fig. 3.3). this displacement allows both mirrors to be recessed as far as possible into the port for optimum beam extraction out of the port and to create the maximum distance between the plasma and the fourth mirror(see 7$^{th}$ critical point above). The final positions of both incidence points on the mirrors are listed in Table 3.1.

| | Center Position (R,z) [mm] | Spot Size [mm] | Distance to next event [mm] | Direction of **k** after event | Direction of **n** of the mirror |
|---|---|---|---|---|---|
| Waveguide | (823.63, 0.0) | 28.604 | 228.52 | 180° | |
| Mirror #1 | (595.11, 0.0) | 30.056 | 129.37(M.3)<br>352.376($\omega_{om}$) | 90° | 45° |
| Mirror #2 | (595.11, 129.37) | 22.7 | 223.01 | 247.5° | 258.75° |
| $\omega_{om}$ | (595.11, 129.37) | 16.0 | 270.53 | 126° | |
| Mirror #3 | (139.14, -59.5) | 25.25 | 144.0(M.4a)<br>254.65($\omega_{op}$) | 126° | 74.25° |
| Mirror #4 ave | (54.5, 57.0) | 22.7 | 85.634 | 235° | 270.5° |
| $\omega_{op}$ | - | 22.2607 | - | - | - |

Table 3.1 X2 antenna mirror data.

The critical points 4 and 5 are used next to approximate the angle of incidence on mirror 3. A line simulating the mirror surface is drawn within the allowable region determined from the above critical points. The incident angle is also forced to bisect the distance between the restriction points 8 and 10. The angle can only be verified after the location and size of the remaining mirrors(1 and 2) and the beam waist between mirrors 2 and 3 have been chosen. The spot size of mirror 2($\omega_2$) is minimized to *22.7mm*. The beam waist is positioned near the corner identified by the 8$^{th}$ critical point. By varying the beam waist size the distances of the waist from both mirrors 1,2 and 3 are altered, which effects the spot size on mirror 1 and the clearances for both critical points 9 and 10. After several iterations a value for the beam waist of *16mm* and a distance of *270.53mm* before mirror 2 is determined as an optimum. With these values the design of the first three mirrors is determined.

The positions and characteristics of each mirror are shown in Table 3.1. Table 3.2 lists the beam characteristics at the resonance layer for the different heating configurations.

| | | X2 Antenna Parameters |
|---|---|---|
| Spot Size $\phi=4*\omega_o$ [cm] | $\kappa=1$ | 10.4 |
| | $\kappa=2$ | 13.4 |
| | $\kappa=3$ | 14.2 |
| Divergence [°] | $\kappa=1$ | 1.5 |
| | $\kappa=2$ | 2.2 |
| | $\kappa=3$ | 2.3 |

Table 3.1 X2 antenna beam characteristics at the heating point.

### 3.1.2 FOURTH MIRROR

Requirements 1 & 2 along with the minimum size in the port (*150mm* diameter) force the fourth mirror to be placed quite close to the plasma. The mirror was chosen to be flat in order to prevent beam distortions which would occur upon rotation of an elliptical mirror. With the mirror rotated to provide the largest poloidal angle, the edge of the mirror is almost flush with the graphite wall tiles. In order to avoid mirror overheating and plasma contamination due to its close proximity to the plasma, it would be advantageous to select a material for mirror 4 which

has a reasonable conductivity, a high melting temperature, and a low sputtering rate. Several candidate materials are listed in Table 3.3 along with their melting points, the ohmic losses assuming worst-case (E-plane) incidence of the beam, the maximum temperature rise on the front surface of the mirror after a *2s* shot assuming no radial conduction and the average steady-state temperature of the mirror assuming a uniform temperature, radiative cooling only and a duty cycle of *0.33%*. (It is assumed that the back surface of the mirror is coated with graphite to increase the average emissivity.) This was obtained from the following equation:

$$T_f = 4s\left(T_o^4 + \frac{P_a}{A\sigma(\varepsilon_{cu} + \varepsilon_b)}\right)^{\frac{1}{4}}, \qquad (3.1)$$

where

$T_f$ = steady state temperature,
$T_o$ = temperature of surrounding material,
$P_a$ = power absorbed in the mirror,
$A$ = Surface area of the mirror
$\sigma$ = thermal conductivity of mirror(?)

| Material | $T_{melt.}$ (°C) | $P_{abs}$ (52°) | Mirror mass (g) | $\Delta T_{max}$ † (°C per shot) | $T_{av}$ (coated) (°C) |
|---|---|---|---|---|---|
| Al | 645 | 0.34% | 142.0 | 366.5 | 100.75 |
| Be | 1285 | 0.41% | 97.0 | 351.5 | 83.12 |
| Cr | 1860 | 0.70% | 378.1 | 679.4 | 137.1 |
| Cu | 1083 | 0.26% | 471.2 | 199.4 | 70.25 |
| Au | 1063 | 0.29% | 1016.0 | 298.6 | 94.15 |
| Mo | 2620 | 0.45% | 541.7 | 471.2 | 113.7 |
| Ni | 1455 | 0.51% | 467.0 | 442.2 | 121.0 |
| Ag | 960.8 | 0.26% | 552.2 | 266.9 | 87.54 |
| Ta | 2950 | 0.70% | 875.6 | 882.3 | 153.4 |
| Ti | 1680 | 1.51% | 236.6 | 2951.3 | 169.4 |
| W | 3370 | 0.47% | 1015.0 | 494.8 | 111.7 |

Table 3.3 Data for mirrors made of different materials for a *0.5MW, 2 s* microwave pulse at *52°* with a duty cycle of *0.33%*.

Both molybdenum and tungsten satisfy the requirements for low sputtering and good thermal properties and could be used as the material for the fourth mirror. Although copper has a

much higher sputtering rate, plasma-facing copper-coated graphite mirrors have been used successfully on DIII-D [13] and this option is also being considered. All other mirrors are made of OFHC copper. Active cooling is not foreseen for all of the mirrors .

### 3.1.3 GENERAL COMMENTS

Although the antenna described here is matched to an *88.9mm* diameter waveguide, modification of mirror 1 would allow matching to waveguide diameters down to *63.5mm*. The final choice of guide diameter will be determined based on the window design of the gyrotrons purchased; the windows being purchased from the gyrotron manufacturer, as mentioned earlier.

The poloidal and toroidal rotations are realized via vacuum feedthroughs. It is envisioned that at least the poloidal rotation is to be adjustable during a shot to optimize power deposition for varying magnetic field and plasma conditions.

The antenna modules greatly exceed the rotation specification 2 in the toroidal direction. This is a result of the system symmetry about the port axis. In fact, there is nothing to prevent the antenna being rotated through 180°. The modules can be used in either the upper lateral or the equatorial ports. The accessibility of the plasma region by the X2 antennas is shown in Fig. 3.4.

### 3.1.4 ANTENNA EFFICIENCY

The efficiency of each mirror is shown in Table 3.4. The overall efficiency for the antenna is 95.5%.

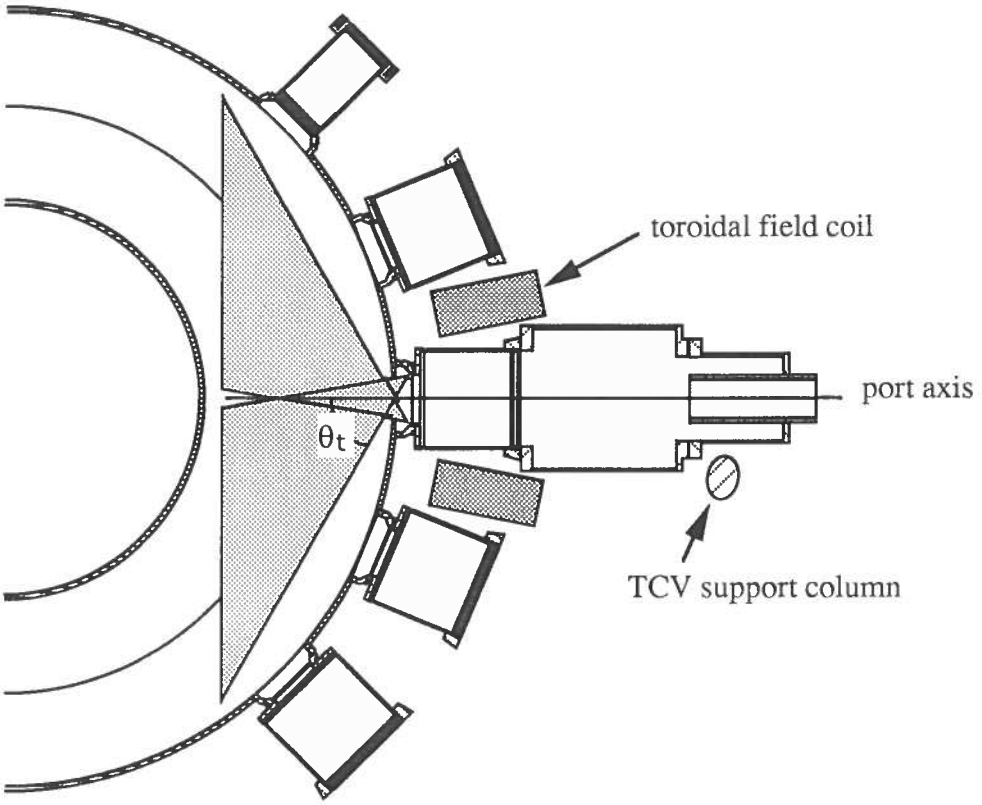


Figure 3.4a View of the toroidal plane with the field coils and support structure shown. The toroidal access area of the X2 antenna is highlighted.

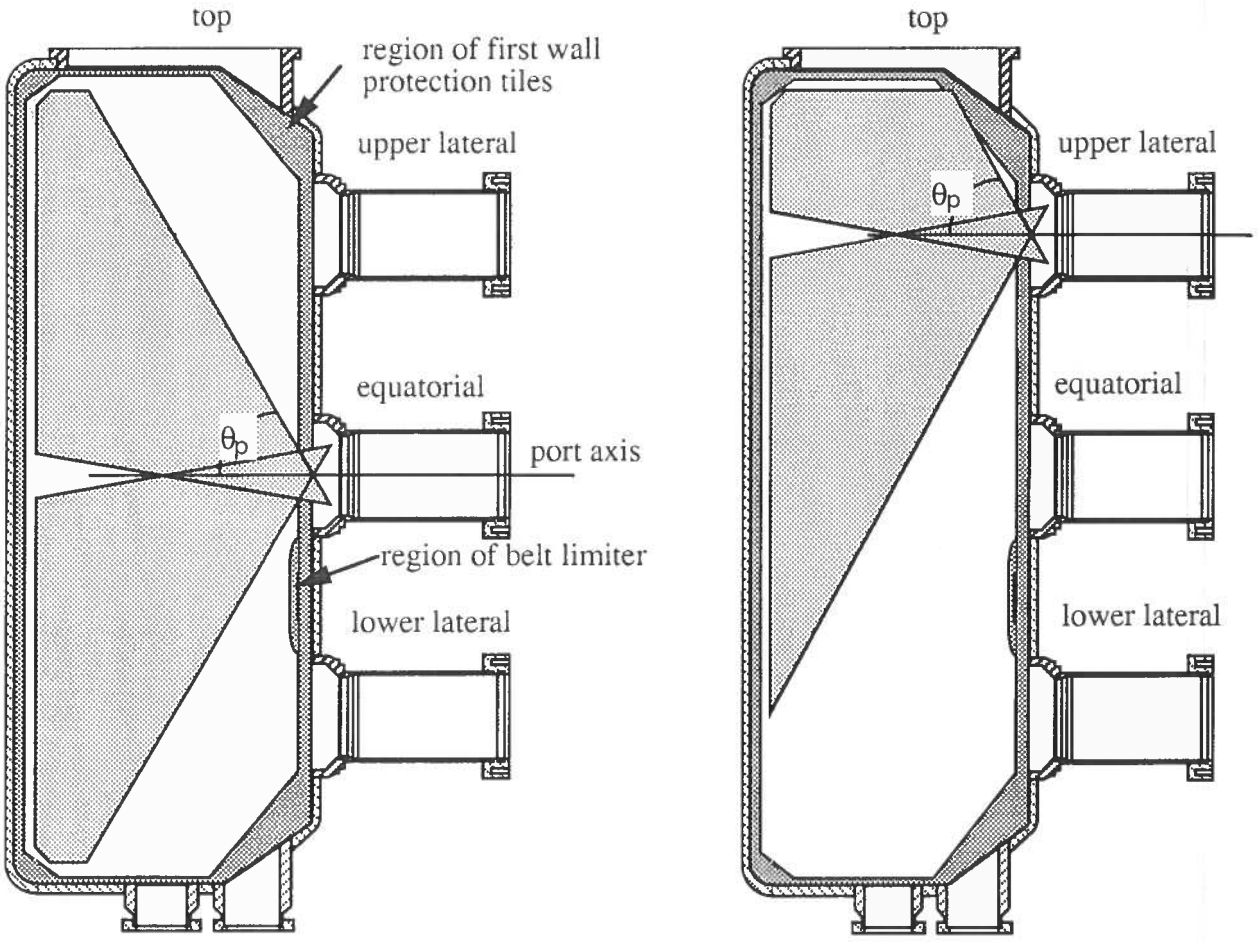


Figure 3.4b Equatorial and upper lateral launch access areas of the X2 antenna.

| | Ohmic Losses | Diff. Losses | Efficiency [%] | Ohmic Losses | Diff. Losses | Total Eff. [%] |
|---|---|---|---|---|---|---|
| Mirror #1 | 0.225% | 0.1% | 99.675 | 0.135% | 0.068% | 99.472 |
| Mirror #2 | 0.192% | 0.1% | 99.708 | | | 99.708 |
| Mirror #3 | 0.257% | 0.1% | 99.643 | 0.268% | 0.134% | 99.241 |
| Mirror #4a | 0.309% | 0.1% | | | | |
| Mirror #4b | 0.496% | 0.1% | | | | |
| Mirror #4 ave | 0.403% | 0.1% | 99.497 | | | 99.497 |
| Total[3] | | | 98.531 | | | 97.793 |

Table 3.4 Total efficiency of the *82.6GHz* antenna.

## 3.2 X3 ANTENNAS

Third Harmonic X-mode (X3) heating will be performed from two large top ports with two beams entering in sector 9, and one in sector 1 (see Fig. 2.1). Due to the larger port size and higher frequency, the antenna system for X3 heating is less complicated than the X2 system. The system has been designed to meet the following requirements:

1 The mirror box must fit between the toroidal field coils.

2 The sector 1 line must be interchangeable with a sector 1 upper-lateral *82.6GHz* line to allow early X3 experiments at reduced field.

3 The beam must have minimum divergence (< 2°, $e^{-2}$ power) at the plasma center for elongations from 1 to 3.

4 A small waist radius (< 30 mm, $e^{-2}$ power) at the heating point must be maintained.

5 The antenna position along the major radius must be flexible: $-a/4 < \Delta R \leq +3a/8$, $\Delta R$ measured about $R=R_0$.

6 The antenna angle must allow aiming of the beam down to the mid plane to -a/2 from the toroidal axis with the mirror at $\Delta R=+3a/8$, and +a/2 with the mirror at $\Delta R=-a/4$.

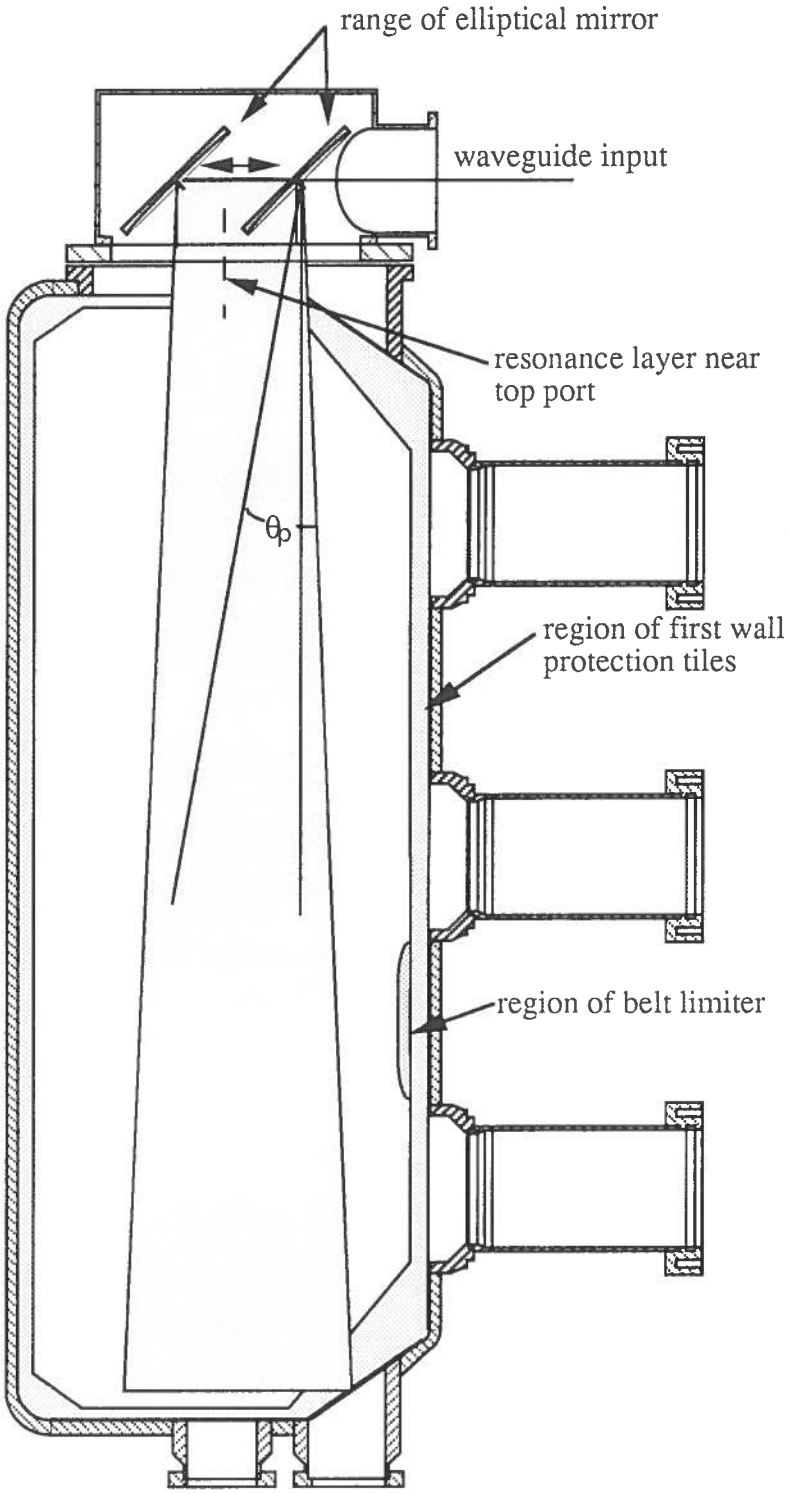


Figure 3.5 Poloidal plane of TCV showing the access area of the X3 antenna.

The combination of radial displacement and poloidal rotation allows the beam to be aimed from either the high or low field side of the X3 resonant surface (see Fig. 3.5), as well as optimal aiming (near tangential) relative to the resonant surface. The radial displacement is also used to prevent the mirror from being positioned on a resonant surface, thus avoiding possible breakdown on the mirror. Early X3 experiments at *82.6GHz* will help to determine whether breakdown is a significant problem, allowing modifications to be made to the X3 launch system if necessary.

A typical design for one of the three antennas of the *118GHz* lines is shown in Fig. 3.6. The requirement that one of the antennas (sector 1) be interchangeable for *82.6GHz* modifies the design slightly. However, since the top port used for the *82.6GHz* experiment has only one input line, the physical constraints are less stringent, allowing a larger mirror size and improved beam characteristics at *118GHz*. Two of the three antennas (T1 and T2.1) utilize a single elliptical mirror to focus the beam into the plasma. The third antenna (T2.2) requires two additional plane mirrors due to physical constraints arising from the toroidal field coils (see Fig. 3.7).

Rotation of the elliptical mirror is controlled by a stepping motor via a vacuum feedthrough and is adjustable during a shot. The permissible mirror rotation is dependent upon its radial position (a typical value is $\pm 6°$). The antenna radial position is manually adjustable on a shot to shot basis. The double input line (sector 9) mirror design allows a displacement of $-a/4 \leq \Delta R \leq +3a/8$, and the interchangeable (*82.6GHz*) antenna in sector 1 allows a mirror displacement of $-a/4 \leq \Delta R \leq +a/2$. Extra pieces of waveguide are added or removed from the end of the line as the mirror is moved radially to maintain approximately the same length between it and the open-ended waveguide (see Fig. 3.6). This ensures proper matching of the spot sizes and focal points. The regions accessible by a typical antenna, considering both the poloidal and radial motion, are shown in Fig. 3.5.

The characteristics of the elliptical mirrors which focuse the beam into the plasma were determined by minimizing the spot size of the beam at the midplane. The beam from the typical *118GHz* antenna has a divergence of $< 1.0°$ and a diameter of $< 86mm$ ($e^{-4}$, power) at the heating point ($z = 60mm$, $k = 2.5$). The average efficiency for the *118GHz* antennas is 0.65%.

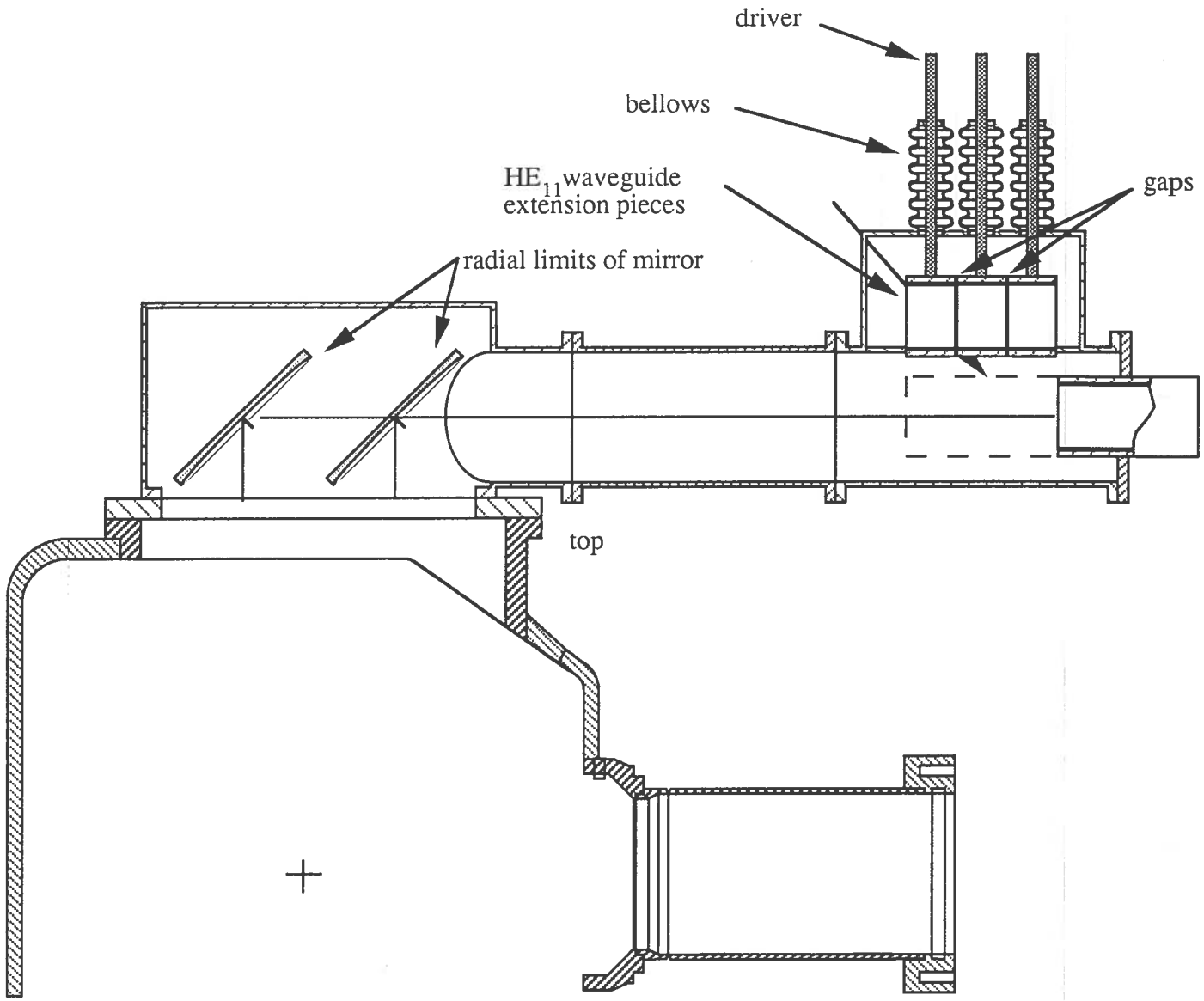


Figure 3.6 Polidal view of the X3 antenna, type T1 and T2.1.

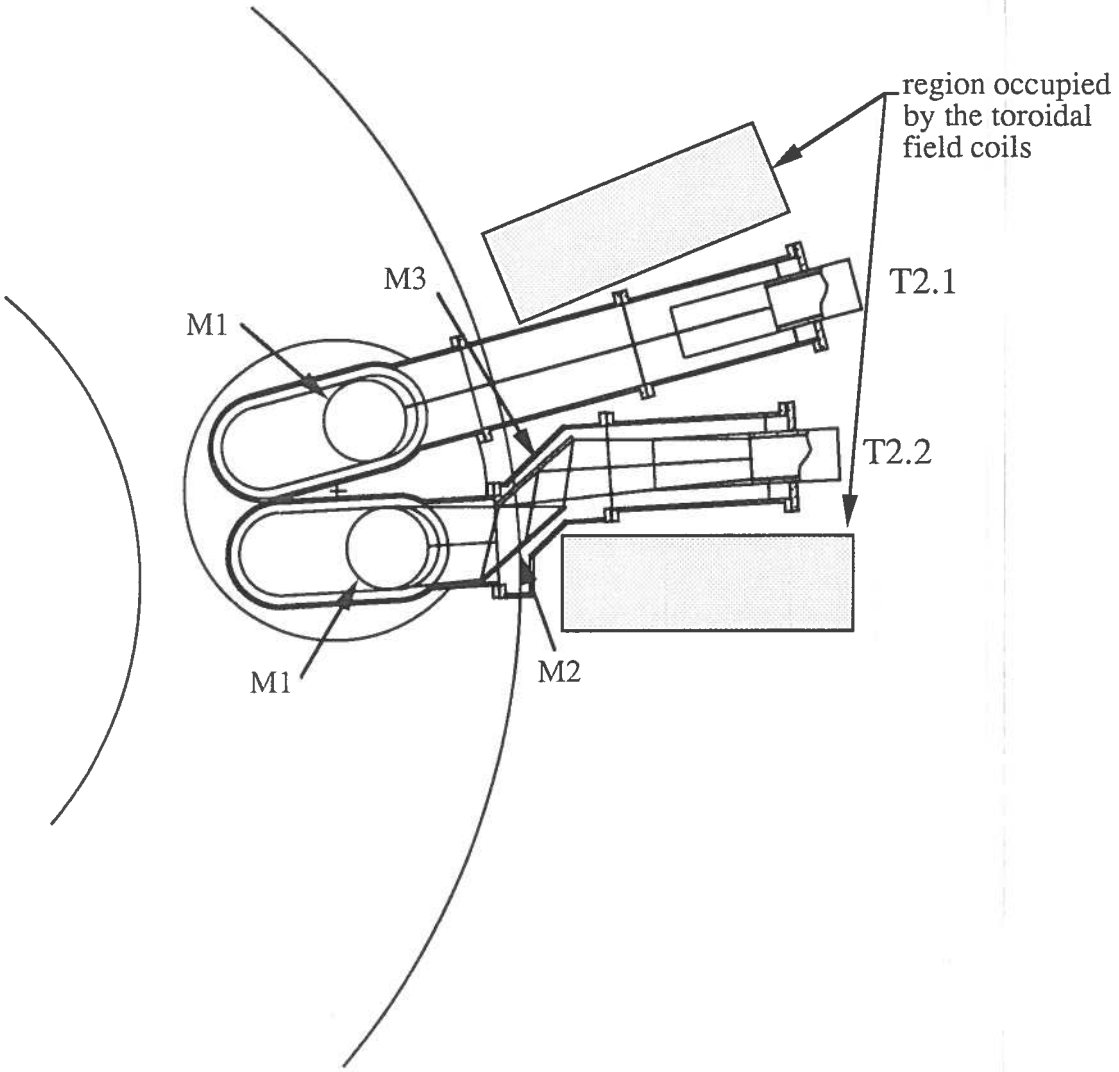


Figure 3.7 Top view of the T2.1 and T2.2 launchers at sector 9. Dotted lines indicate location of the HE11 extension pieces.

## 4 TOTAL TRANSMISSION EFFICIENCY

The efficiency of the individual components of both transmission lines (*82.6GHZ* and *118GHz*) is shown in Table 4.1a and b for the two possible waveguide diameters. The over all efficiency of the X2 lines is expected to be over 88% and over 90% for the X3.

| | 82.6 GHz | | | 118 GHz | | |
|---|---|---|---|---|---|---|
| Component | % Loss per item | # of items | Effi-ciency [%] | % Loss per item | # of items | Effi-ciency [%] |
| $HE_{11}$ coupling mirror[1] | 0.33 | 1 | 99.67 | 0.37 | 1 | 99.63 |
| $HE_{11}$ coupling | 2.0 | 1 | 98.00 | 2.0 | 1 | 98.00 |
| $HE_{11}$ waveguide [dB/m] | 9.15E-5 | 30m | 99.94 | 8.98E-5 | 30m | 99.94 |
| $HE_{11}$ waveguide misalignment | ~1 | – | 99.00 | ~1 | – | 99.00 |
| Miter bend[2] | 0.51 | 2 | 98.98 | 0.40 | 2 | 99.20 |
| Miter bend polarizer | 0.91 | 2 | 98.19 | 0.67 | 2 | 98.66 |
| Expansion joints | 0.03 | 2 | 99.95 | 0.02 | 2 | 99.97 |
| Vacuum window[3] | ~2 | 1 | 98.00 | ~2 | 1 | 98.00 |
| Gate valve | 0.05 | 2 | 99.91 | 0.03 | 2 | 99.95 |
| Open ended waveguied | 2.0 | 1 | 98.00 | 2.0 | 1 | 98.00 |
| Antenna[4] | 1.47 | 1 | 98.53 | 0.65 | 1 | 99.35 |
| Total | | | 88.75 | | | 90.14 |

1 Includes 0.1% loss due to diffraction.

2 Includes 0.537% (0.301%) due to mode conversion for *82.6GHz* ( *118GHz*).
With H-plane bends the losses are 2.58% (2.18%) at *82.6GHz* (*118GHz*).

3 Actual losses dependent upon window type chosen.

4 The average loss for the three *118GHz* antenna designs is used.

Table 3.5a Total transmission line loss for *82.6GHz* and *118GHz* (a=*44.45mm*).

| Component | 82.6 GHz | | | 118 GHz | | |
|---|---|---|---|---|---|---|
| | % Loss per item | # of items | Effi-ciency [%] | % Loss per item | # of items | Effi-ciency [%] |
| $HE_{11}$ coupling mirror[1] | 0.33 | 1 | 99.67 | 0.37 | 1 | 99.63 |
| $HE_{11}$ coupling | 2.0 | 1 | 98.00 | 2.0 | 1 | 98.00 |
| $HE_{11}$ waveguide [dB/m] | 2.50E-4 | 30m | 99.83 | 2.46E-4 | 30m | 99.83 |
| $HE_{11}$ waveguide misalignment[2] | ~0 | – | 100.00 | ~0 | – | 100.00 |
| Miter bend[3] | 0.68 | 2 | 98.55 | 0.53 | 2 | 98.94 |
| Miter bend polarizer | 1.35 | 2 | 97.32 | 0.93 | 2 | 98.15 |
| Expansion joints | 0.08 | 2 | 99.85 | 0.04 | 2 | 99.92 |
| Vacuum window[4] | ~2 | 1 | 98.00 | ~2 | 1 | 98.00 |
| Gate valve | 0.13 | 2 | 99.74 | 0.08 | 2 | 99.85 |
| Open ended waveguied | 2.0 | 1 | 98.00 | 2.0 | 1 | 98.00 |
| Antenna[5] | 1.47 | 1 | 98.53 | 0.65 | 1 | 99.35 |
| Total | | | 88.13 | | | 90.11 |

1 Includes 0.1% loss due to diffraction.

2 Negligable losses for mwaveguide missalignments.

3 Includes 0.537% (0.301%) due to mode conversion for *82.6GHz* ( *118GHz* ). With H-plane bends the losses are 2.58% (2.18%) at *82.6GHz* (*118GHz* ).

4 Actual losses dependent upon window type chosen.

5 The average loss for the three *118GHz* antenna designs is used.

Table 3.5b Total transmission line loss for *82.6GHz* and *118GHz* (a=*31.75mm*).

ACKNOWLEDGMENTS

We would like to acknowledge Jean-Claude Magnin for the helpful discussions in the design of the X2 and X3 antennas.

## REFERENCES


[1] W. Henle et al., EUR-FU/80/90-99.

[2] ECRH-Group: W. Kasparek et al. Final Report Contract-No 419/90-4/FU-D NET.

[3] L. Rebuffi,Gaussian Beam Matching to a Hybrid Mode Waveguide, The NET Team, c/o Max Planck Inst. Feur Plasmaphysik, Boltzmanstr. 2, D-8046 Garching, FRG, (1991).

[4] P. Goldsmith, "Qausi-optical techniques at Millimtre and Submillimetre Wavelengths", Ch. 5 in *Infared and Millimetre Waves* Vol 6. K. Button Ed. Academic Press (1982).

[5] P. Belland and J.P. Crenn, Appl. Optics, **21** (1982) 522.

[6] C. Moeller et al., 18th Fusion Berlin 1991, Vol 15C Part III, (1991) 369.

[7] J. Doane, Infared and Millimeter Waves, **13** (1985) p.123.

[8] D. Wagner, M. Thumm, W. Kasparek, 15th Int. Conf. on IR&MM Waves, Orlando 1990, Proc. SPIE 1514, p. 437.

[9] R.B. Vaganov, Radio Eng. Electron Physics, **18** (1973) p.170.

[10] J. Doane, Int.J. of Inf. and MM Waves, Vol. 13, No. 11 (1992) 1727.

[11] Felix M.A. Smits, in Proc. 7th Joint Workshop on ECE and ECRH (Hefei, China, 1989).

[12] M.Q.Tran, et al., LRP 458/92.

[13] R.W. Callis, General Atomics, private communication.